SCIENCE CHINA PRESS

SCIENCE CHINA Life Sciences
life.scichina.com link.springer.com
https://doi.org/10.1007/s11427-023-2434-8

RESEARCH PAPER

Targeting lncRNA16 by GalNAc-siRNA conjugates facilitates chemotherapeutic sensibilization via the HBB/NDUFAF5/ROS pathway

Yanfang Liu[1†], Yan Wang[2†], Bing Liu[1], Wenzhong Liu[2], Yuanyuan Ma[1], Yiren Cao[2], Shi Yan[1], Panpan Zhang[3], Lixin Zhou[4], Qimin Zhan[2,5,6*] & Nan Wu[1*]

[1]Key Laboratory of Carcinogenesis and Translational Research (Ministry of Education/Beijing), Department of Thoracic Surgery II, Peking University Cancer Hospital and Institute, Beijing 100142, China;
[2]Key Laboratory of Carcinogenesis and Translational Research (Ministry of Education/Beijing), Laboratory of Molecular Oncology, Peking University Cancer Hospital and Institute, Beijing 100142, China;
[3]Key Laboratory of Carcinogenesis and Translational Research (Ministry of Education/Beijing), Department of Thoracic Oncology II, Peking University Cancer Hospital and Institute, Beijing 100142, China;
[4]Key Laboratory of Carcinogenesis and Translational Research (Ministry of Education), Department of Pathology, Peking University Cancer Hospital and Institute, Beijing 100142, China;
[5]Peking University International Cancer Institute, Beijing 100191, China;
[6]Institute of Cancer Research, Shenzhen Bay Laboratory, Shenzhen 518132, China

†Contributed equally to this work
*Corresponding authors (Qimin Zhan, email: zhanqimin@bjmu.edu.cn; Nan Wu, email: nanwu@bjmu.edu.cn)

Received 29 June 2023; Accepted 19 July 2023; Published online 19 December 2023

Chemoresistance is a significant barrier to effective cancer treatment. Potential mechanisms for chemoresistance include reactive oxygen species (ROS) accumulation and expression of chemoresistance-promoting genes. Here, we report a novel function of lncRNA16 in the inhibition of ROS generation and the progression of chemoresistance. By analyzing the serum levels of lncRNA16 in a cohort of 35 patients with non-small cell lung cancer (NSCLC) and paired serum samples pre- and post-treatment from 10 NSCLC patients receiving neoadjuvant platinum-based chemotherapy, performing immunohistochemistry (IHC) assays on 188 NSCLC tumor samples, using comprehensive identification of RNA-binding proteins by mass spectrometry (ChIRP-MS) assays, as well as RNA immunoprecipitation (RIP) and RNA pull-down analyses, we discovered that patients with increased serum levels of lncRNA16 exhibited a poor response to platinum-based chemotherapy. The expression of hemoglobin subunit beta (HBB) and NDUFAF5 significantly increases with the development of chemoresistance. LncRNA16 binds to HBB and promotes HBB accumulation by inhibiting autophagy. LncRNA16 can also inhibit ROS generation via the HBB/NDUFAF5 axis and function as a scaffold to facilitate the colocalization of HBB and NDUFAF5 in the mitochondria. Importantly, preclinical studies in mouse models of chemo-resistant NSCLC have suggested that lncRNA16 targeting by trivalent N-acetylgalactosamine (GalNAc)-conjugated siRNA restores chemosensitivity and results in tumor growth inhibition with no detectable toxicity *in vivo*. Overall, lncRNA16 is a promising therapeutic target for overcoming chemoresistance, and the combination of first-line platinum-based chemotherapy with lncRNA16 intervention can substantially enhance anti-tumor efficacy.

chemoresistance | lncRNA | RNA interference | ROS | chemosensitizer

INTRODUCTION

Chemotherapy, one of the most important cancer treatment strategies, has been widely applied to cancer treatment (Zhang et al., 2022a). Platinum-based chemotherapy is a first-line systemic therapy for lung, metastatic urothelium, and ovarian cancers (Galsky et al., 2011; Hanna et al., 2017; Pignata et al., 2017). Compared with surgery alone, platinum-based chemotherapy remarkably improves survival time and reduces the risk of death in patients with cancer (NSCLC Meta-analysis Collaborative Group, 2014). For 36%–72% of non-small cell lung cancer (NSCLC), ~70%–80% of epithelial ovarian cancer, and ~50% of bladder cancer, however, a large proportion of patients experience chemoresistance, side effects, and relapse (Cathomas et al., 2022; Galsky et al., 2011; Pignata et al., 2017; Wang et al., 2017), leading to an urgent need to seek novel strategies. The development of chemoresistance is closely associated with reduced reactive oxygen species (ROS) accumulation, expression of chemoresistance-promoting genes, and enhanced oxidative phosphorylation in the mitochondria (Bhola et al., 2013; Choi et al., 2020; Lee et al., 2017). Evidence has shown that the activity of antioxidant enzymes usually increases in chemo-resistant cancer cells, decreasing ROS levels and further inhibiting cell apoptosis (Xu et al., 2022). Cytoprotective antioxidation has become an obstacle to effective anti-tumor treatment. Therefore, identifying new targets to upregulate ROS levels is an emerging strategy for overcoming chemoresistance.

Long non-coding RNAs (lncRNAs) are a class of non-coding RNA (ncRNAs) longer than 200 nt and lack open reading frames (Zhang et al., 2023). LncRNAs are abnormally expressed in cancers and are closely related to an increased risk of cancer metastasis (Gupta et al., 2010; Shah and Sukumar, 2010). As the most abundant type of regulatory RNA, lncRNAs are widely distributed in extracellular vesicles, peripheral serum, saliva, urine, and other bodily fluids (He et al., 2021; Matsui and Corey, 2017), indicating the superior potential of lncRNA interference

and the necessity of developing effective lncRNA intervention targets. Our previous study used a custom microarray platform to construct lncRNA expression profiles in tumors and paired adjacent normal tissues from 76 patients (20 with gastric cancer, 20 with colon cancer, 16 with liver cancer, and 20 with lung cancer). We identified 157 abnormally expressed lncRNAs and validated them through reverse transcription PCR (RT-qPCR). Among them, lncRNA16 was differentially expressed only in lung cancer, whereas the other 156 lncRNAs were dys-regulated in at least two cancer types (Yuan et al., 2016). In addition, we found that lncRNA16 contributes to tumor growth, acts as a potential biomarker for the diagnosis of early-stage NSCLC, and is a potential therapeutic target for NSCLC treatment (Zhu et al., 2017). However, it remains unclear whether lncRNA16 promotes drug resistance.

Here, we report a novel function of lncRNA16 in the progression of chemoresistance. LncRNA16 inhibited ROS accumulation via the hemoglobin subunit beta (HBB)/NDUFAF5 pathway. We also investigated the effects of lncRNA16 knockdown with siRNA using trivalent N-acetylgalactosamine (GalNAc) as the carrier. GalNAc-silncRNA16 (named Nano-silncRNA16) clearly inhibits tumor growth and enhances the therapeutic efficacy of cancer cells *in vitro* and *in vivo*, indicating its potential as a treatment strategy for chemoresistance.

RESULTS

High level of lncRNA16 is related to chemoresistance

Considering the critical role of platinum-based chemotherapy in cancer treatment, the correlation between lncRNA16 levels and the response to platinum-based chemotherapy was assessed. Interestingly, non-responsive patients exhibited higher serum levels of lncRNA16 than responsive patients (P=0.0023) (Figure 1A). To analyze the dynamic expression of lncRNA16 in response to platinum-based therapy, we collected paired serum samples pre- and post-treatment from 10 patients with NSCLC receiving neoadjuvant platinum-based chemotherapy, including five responders and five non-responders. Importantly, the comparison between pre- and post-treatment serum lncRNA16 levels showed that after chemotherapy, lncRNA16 levels in the non-responsive group remained almost unchanged (Figure 1B), and a significant increase in lncRNA16 levels was observed among the five patients in the non-responsive group (Figure 1B), indicating that lncRNA16 enhanced chemoresistance. RT-qPCR was performed to compare lncRNA16 levels in A549 and cisplatin-resistant A549 (A549/DDP) cells. Interestingly, the lncRNA16 levels were significantly higher in A549/DDP cells (Figure 1C). Overexpression of lncRNA16 in A549 cells caused an approximately 4.40-fold increase in the IC50 of cisplatin (DDP) (Figure S1A in Supporting Information). In contrast, the knockdown of lncRNA16 induced a 7.08-fold decrease in the IC50 of DDP in the A549/DDP cells (Figure S1B in Supporting Information), indicating that high lncRNA16 expression enhances the resistance of A549 cells to DDP. MTS assays were performed to confirm that lncRNA16 enhanced DDP resistance. The results indicated that sensitivity to DDP was significantly increased when lncRNA16 was knocked down in A549/DDP cells (Figure 1D), causing substantial inhibition of cell proliferation (Figure 1D). In contrast, lncRNA16 overexpression facilitated the proliferation of A549 cells, with or without DDP treatment (Figure 1E). In addition, lncRNA16 knockdown promoted DDP sensitivity, which was further confirmed by colony formation assays (Figure 1F–G). To further demonstrate that lncRNA16 facilitates chemoresistance, lncRNA16 expression was investigated in several other cisplatin-resistant NSCLC cell lines. The results showed that H460/DDP, H520/DDP, and H226/DDP cells exhibited higher lncRNA16 levels than their chemo-sensitive parental cell lines (Figure S2A in Supporting Information). H460/DDP and H520/DDP cells were used to verify the function of lncRNA16 in contributing to chemoresistance. As expected, lncRNA16 overexpression promoted proliferation and DDP resistance in H520 and H460 cells (Figure S2B and C in Supporting Information), whereas lncRNA16 knockdown inhibited cell growth and enhanced DDP sensitivity in H520/DDP and H460/DDP cells (Figure S2D and E in Supporting Information). This was further verified by colony formation assays (Figure S2F–I in Supporting Information). Additionally, lncRNA16 had almost no effect on cell invasion or migration (Figure S3 in Supporting Information). These results revealed that high levels of lncRNA16 are related to chemoresistance and that lncRNA16 promotes DDP resistance.

LncRNA16 binds to HBB and enhances HBB accumulation via autophagy

Increasing evidence has shown that RNA-binding proteins (RBPs) play key roles in lncRNA-mediated chemoresistance and tumor progression (Shi et al., 2020). To reveal proteins binding to lncRNA16, comprehensive identification of RNA-binding proteins by mass spectrometry (ChIRP-MS) was performed, and five proteins, including hemoglobin subunit alpha (HBA1), HBB, lipocalin-1 (LCN1), SNC73 (IgHα1), and GAPDH, were identified (Figure 2A). The results indicated the highest enrichment in HBB. Additionally, the RNA immunoprecipitation (RIP) assay indicated significant enrichment of lncRNA16 in the immunoprecipitation of HBB (Figure S4 in Supporting Information) (SNC73 was excluded because there were no corresponding commercial antibodies). Therefore, HBB was selected for further studies. Western blotting revealed that HBB protein levels were higher in A549/DDP cells than in A549 cells (Figure 2B). Knockdown or overexpression of lncRNA16 also significantly affected HBB expression, indicating that lncRNA16 binds to and regulates HBB protein levels (Figure 2B). HBB is involved in Fe^{3+} and oxygen transport (Pillai et al., 2020), and structural mutations or abnormal enrichment of HBB leads to hemoglobin dysfunction, sickle cell disease, and thalassemia (Newby et al., 2021). Recently, HBB was found to perform other functions, such as oxygen sensing, ROS scavenging, and iron metabolism regulation (Zheng et al., 2017). LncRNA16 is located on human chromosome 11q12.3, is composed of six exons with a full length of 240 nt, and spanned nearly 1.60 kilobases (kb). To further explore the specific segment of lncRNA16 that binds to HBB, the secondary structure of lncRNA16 was analyzed using the online tool RNAFOLD. This tool provides two predicted structures: a minimum free-energy structure (Figure S5A in Supporting Information) and a centroid secondary structure (Figure S5B in Supporting Information). Based on the similarity between the two structures, the two sequences were named lncRNA16 domains (RD) (Figure S5A and B in Supporting Information). Therefore, lncRNA16 was divided into four truncation regions: T1, T2, T3 and T4 (Figure 2C). RNA pull-down analysis showed

https://doi.org/10.1007/s11427-023-2434-8

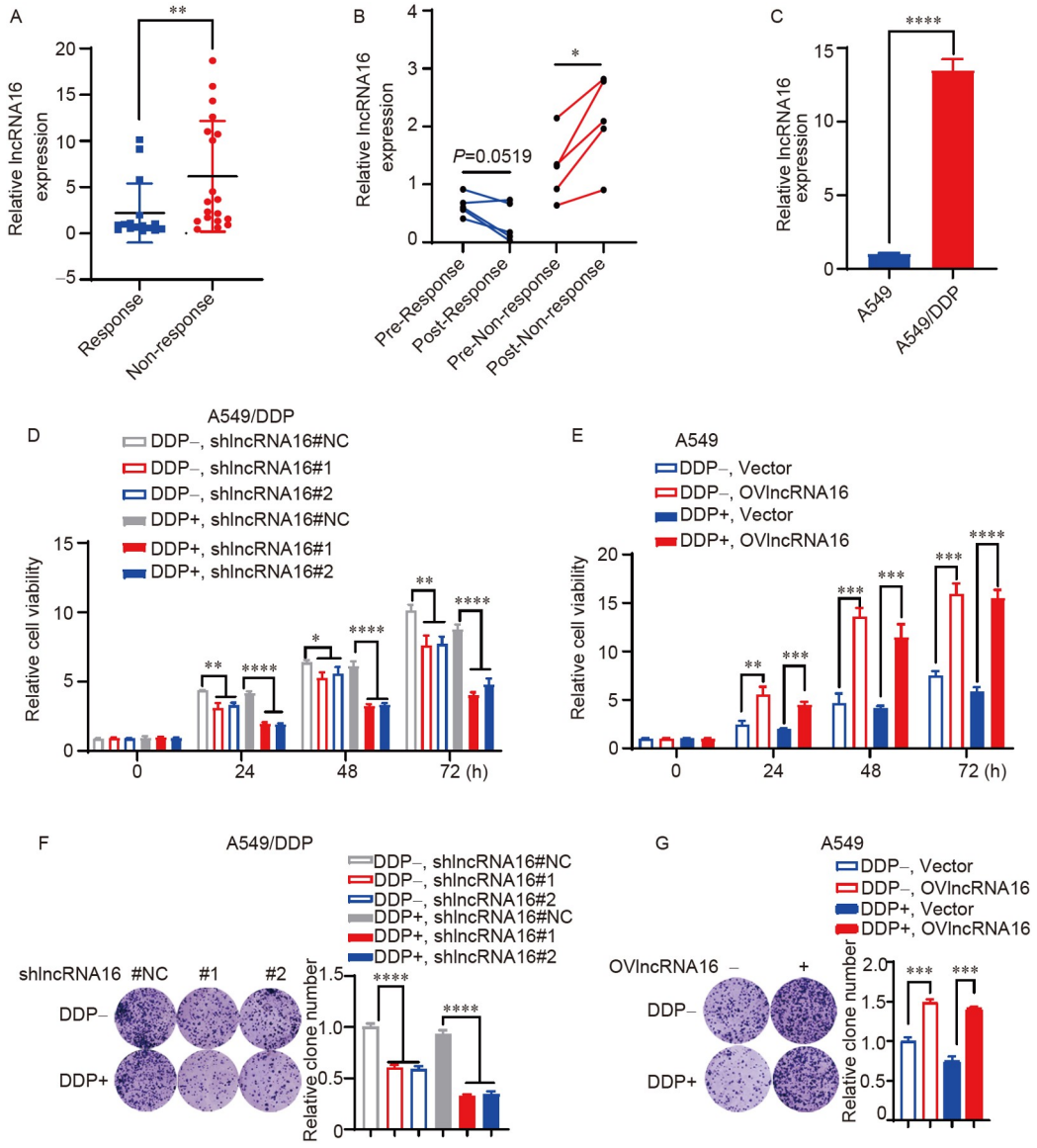

Figure 1. High level of lncRNA16 is related to chemoresistance. A, The pre-treatment serum lncRNA16 levels were compared among the response (n=16) and non-response (n=19) NSCLC patients. B, The pre- and post-treatment serum lncRNA16 levels were investigated among the response (n=5) and non-response (n=5) NSCLC patients. C, Expression of lncRNA16 in A549 and A549/DDP cells was compared via RT-qPCR analysis. D and E, MTS assays were performed to show cell growth at 0, 24, 48, and 72 h. F and G, Colony formation assays were performed to show cell proliferation capability. For A, statistical significance was calculated with the Mann-Whitney U-test; For B, statistical significance was calculated with the paired t-test. For D and E, statistical significance was calculated with two-way ANOVA. For F and G, statistical significance was calculated with one-way ANOVA. *, P<0.05; **, P<0.01; ***, P<0.001; ****, P<0.0001.

that lncRNA16 binds to HBB through T1, T2, and T4 (Figure 2D). Furthermore, 3D views of the binding between lncRNA16 and HBB were analyzed using nucleotide-protein docking. The results showed that lncRNA16 bound tightly to HBB (Figure 2E), with an extremely low binding energy of −1,194.646 kcal mol^{-1}. In addition, the T1, T2, and T4 segments of lncRNA16 bound to HBB, whereas T3 (marked as green) did not (Figure 2E). Furthermore, a combination of fluorescence *in situ* hybridization (FISH) and immunofluorescence (IF) assays suggested that HBB and lncRNA16 were mainly located in the cytoplasm (Figure S6 in Supporting Information); furthermore, lncRNA16 and HBB were colocalized in the cytoplasm (Figure 2F; Figure S7A in Supporting Information).

In eukaryotic cells, proteins are degraded mainly via autophagy or the proteasomal pathway (Gwon et al., 2021). A549/DDP cells were treated with the proteasome inhibitor MG132 to determine the mechanism of HBB degradation. Interestingly, the HBB protein level did not increase compared with that in the DMSO group (Figure 2G), indicating that HBB was not degraded via the proteasome pathway. To verify whether HBB was degraded by autophagy, increasing concentrations of the autophagy inhibitor chloroquine (CQ) were added. As expected, HBB protein levels increased with increasing CQ concentrations (Figure 2H). In addition, the treatment of A549/DDP cells with rapamycin (an autophagy activator) resulted in a pronounced reduction in HBB protein levels (Figure 2I). To determine whether lncRNA16 affects HBB protein levels by regulating autophagy, the effects of lncRNA16 on autophagy were examined. Interestingly, knockdown or overexpression of lncRNA16 caused a corresponding increase or decrease in

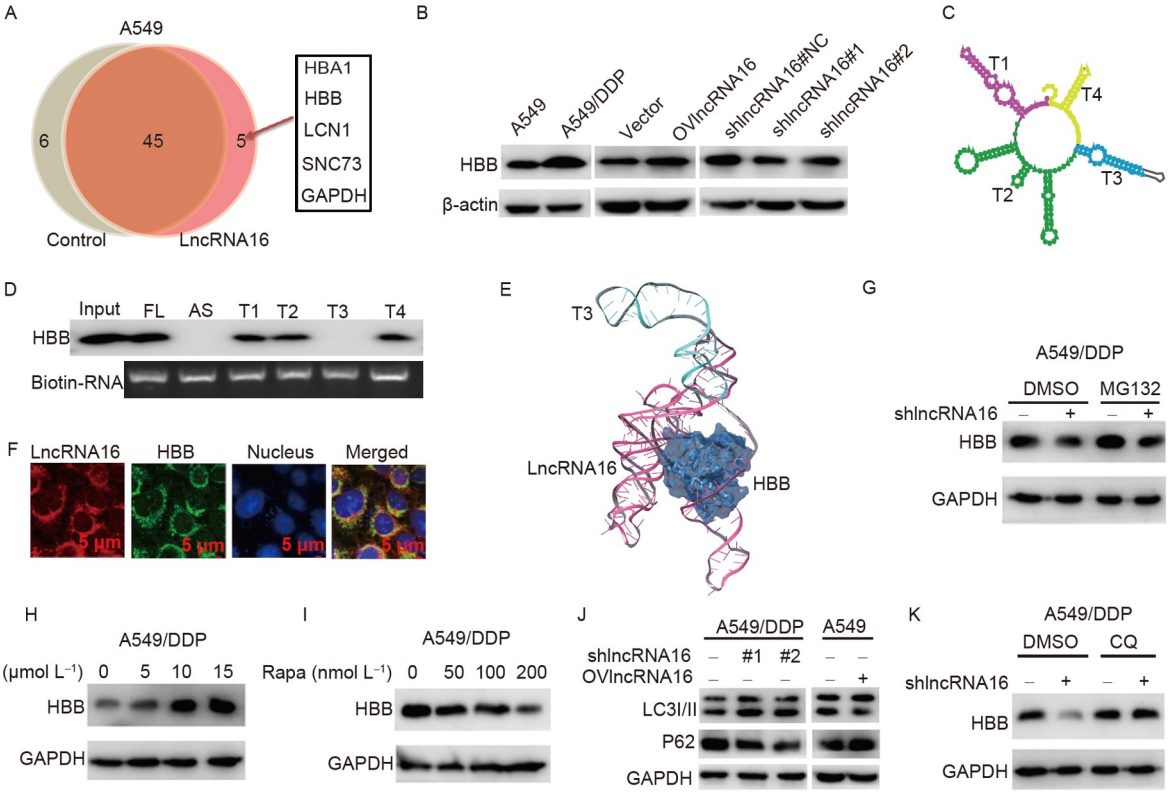

Figure 2. LncRNA16 binds with HBB and promotes accumulation of HBB via autophagy. A, The proteins bound to lncRNA16 were detected by ChIRP-MS technology in lncRNA16 over-expressed A549 cells. B, Effects of lncRNA16 on HBB protein levels were investigated through Western blots. C, The secondary structure of lncRNA16 was predicted through RNAFOLD. D, RNA pull-down assay was performed to detect the specific region of lncRNA16 binding to HBB. The input was used as a positive control. FL and AS represented the sense and antisense strands of lncRNA16, respectively. E, The 3D views of binding between lncRNA16 and HBB. The T3 segment of lncRNA16 was marked as green. F, FISH and IF assay were combined to show the colocalization of lncRNA16 and HBB in A549/DDP cells. G, Western blotting was performed to detect the effects of MG132 and lncRNA16 knockdown on HBB protein levels. H and I, Western blot was performed to detect the effects of activating or inhibiting autophagy on HBB protein levels. The A549/DDP cells were treated with an increased concentration of autophagy inhibitor CQ or autophagy activator rapamycin (Rapa). J, Western blot was performed to detect the effects of lncRNA16 on autophagy. K, Western blot was performed to detect the effects of the combination of lncRNA16 knockdown with autophagy inhibition on HBB protein levels.

autophagy, respectively (Figure 2J), suggesting an inhibitory effect of lncRNA16 on autophagy. Additionally, treatment with CQ reversed HBB inhibition caused by lncRNA16 knockdown (Figure 2K), corroborating that lncRNA16 contributes to HBB accumulation by inhibiting autophagy.

LncRNA16 inhibits ROS production and enhances chemoresistance via HBB

HBB inhibits ROS-mediated cytotoxicity and protects cells from oxidative damage (Li et al., 2013; Zheng et al., 2017). To determine whether lncRNA16 and HBB regulate ROS levels in A549/DDP cells, MitoSOX was used to label the ROS. As expected, ROS levels significantly decreased in both A549/DDP cells and lncRNA16-overexpressed A549 cells compared to the control cells (Figure 3A and B). In contrast, ROS levels were upregulated in lncRNA16 and HBB knocked-down cells (Figure 3C and D), indicating that lncRNA16 and HBB are involved in ROS regulation. Additionally, lncRNA16 knockdown increased the ROS levels, which was attenuated by HBB overexpression (Figure 3E). Conversely, lncRNA16 overexpression resulted in a remarkable decrease in ROS levels, which was reversed by HBB knockdown (Figure 3E), suggesting that lncRNA16 inhibited ROS levels through HBB.

To gain a better understanding of HBB in chemoresistance in clinics, we first performed a retrospective analysis of 34 treatment-naïve NSCLC patients in The Cancer Genome Atlas (TCGA) dataset, who subsequently received platinum-based chemotherapy, and were divided into two groups according to their response to treatment. A significant difference was observed in HBB mRNA levels between the two groups at baseline (P=0.0079) (Figure S8 in Supporting Information). Furthermore, to investigate how HBB responds to platinum-based chemotherapy, we retrospectively collected 188 cancer samples from 47 patients with NSCLC using endoscopic biopsy and surgery at pre-treatment (baseline) and post-treatment time points, respectively. Among them, 20 responded well to platinum-based chemotherapy, whereas the other 27 showed resistance to therapy. Immunohistochemistry (IHC) analyses showed almost no difference in HBB protein levels at baseline between the response and non-response groups; however, after treatment, the non-response group showed higher HBB levels (Figure 3F). After receiving platinum-based chemotherapy, HBB levels dramatically decreased in the responsive group, whereas HBB protein levels increased in the non-responsive group, which caused remarkable post-treatment differences between the two groups (Figure 3F), suggesting that HBB changes with chemoresistance and is associated with platinum resistance. MTS assay was performed to assess the effect of HBB on DDP resistance. HBB knockdown significantly decreased the cell viability at 24, 48,

https://doi.org/10.1007/s11427-023-2434-8

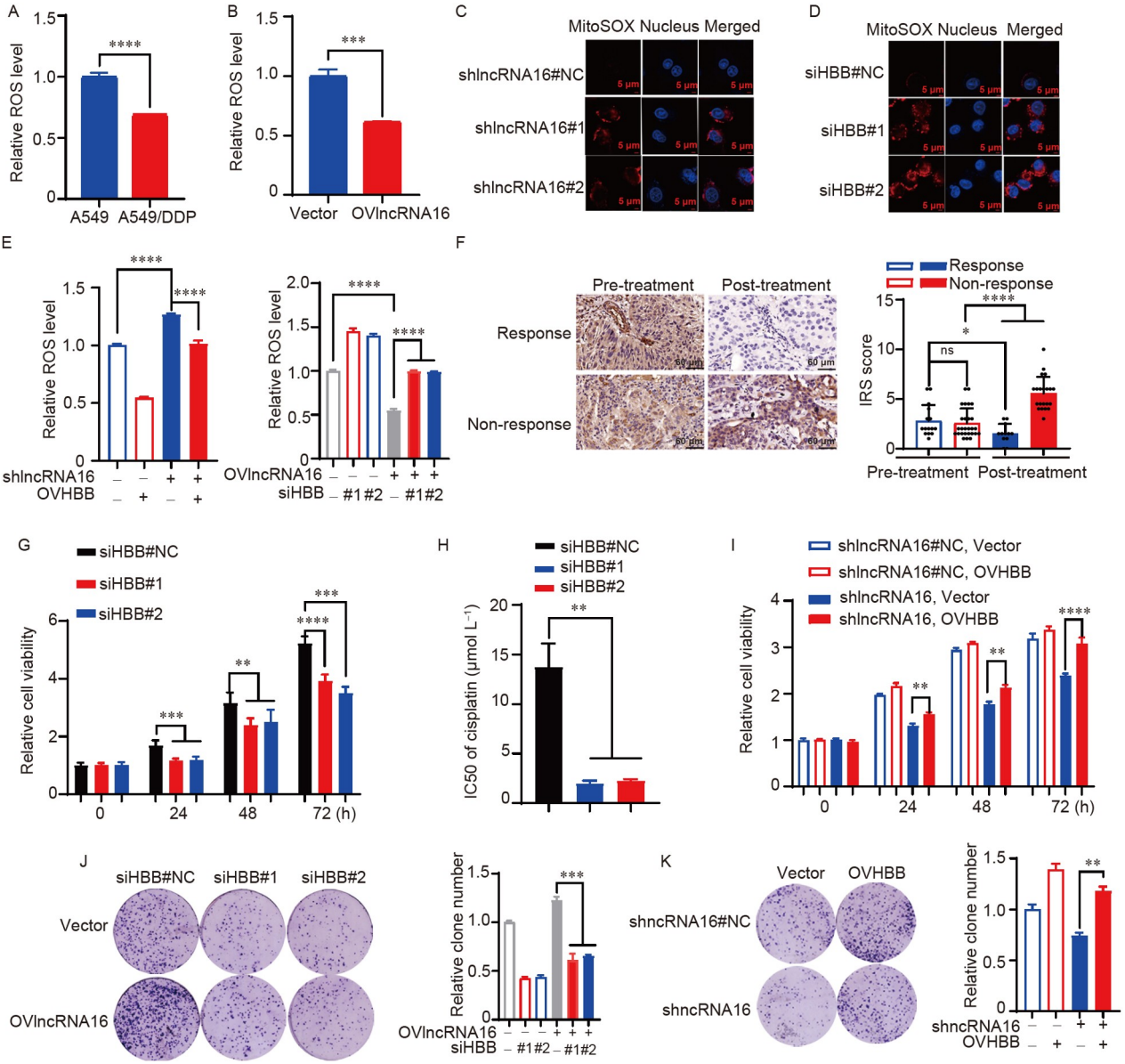

Figure 3. LncRNA16 promotes DDP resistance and inhibits ROS via HBB. A, ROS levels detected in A549 and A549/DDP cells. B, Detection of the effects of overexpression of lncRNA16 on ROS levels in A549 cells. C, MitoSOX was used to label ROS. ROS detection was performed to investigate the effects of lncRNA16 knockdown on ROS levels. D, ROS detection was performed to investigate the effects of HBB knockdown on ROS levels. E, Rescue experiments were performed to investigate whether lncRNA16 inhibited ROS levels through HBB. F, IHC analyses were performed to detect pre-treatment and post-treatment HBB protein changes among 47 NSCLC patients. G, MTS assays were performed to investigate the effects of HBB knockdown on cell proliferation in A549/DDP cells. H, IC50 detection was performed to investigate the effects of HBB knockdown on DDP sensitivity in A549/DDP cells. I, Rescue experiments investigated whether lncRNA16 contributed to cell proliferation via HBB. J and K, Rescue analyses were performed to investigate whether lncRNA16 contributed to colony formation via HBB. Statistical significance was calculated with Student's *t*-test for A and B. For E and H, statistical significance was calculated with one-way ANOVA. For F, statistical significance was calculated with the Mann-Whitney *U*-test. For G, I–K, statistical significance was calculated with two-way ANOVA (*, $P<0.05$; **, $P<0.01$; ***, $P<0.001$; ****, $P<0.0001$; ns, non-significance).

and 72 h (Figure 3G). Moreover, HBB knockdown caused an approximately 5.42-fold decrease in the IC50 of DDP in A549/DDP cells (Figure 3H), indicating that HBB contributed to DDP resistance. MTS experiments were performed to confirm that lncRNA16 promoted DDP resistance via HBB, and the results revealed that HBB overexpression relieved the inhibition of proliferation caused by lncRNA16 knockdown within 24 h (Figure 3I). Furthermore, the colony formation assay suggested that HBB knockdown inhibited the cell growth-promoting function caused by lncRNA16 overexpression (Figure 3J), whereas lncRNA16 knockdown followed by HBB overexpression showed the opposite results (Figure 3K). Collectively, lncRNA16 inhibits ROS production and enhances A549 DDP resistance via HBB.

LncRNA16 acts as a scaffold to facilitate the binding of HBB and NDUFAF5

Mitochondrial oxidative respiration is the primary source of ROS, which is generated by mitochondrial complexes I (CI) and III (CIII) (West et al., 2011). Based on these results, we speculate that lncRNA16 and HBB may regulate ROS levels in the

mitochondria. Subsequently, protein binding to HBB was analyzed using an online tool (http://gpsprot.org/). Interestingly, the results demonstrated that HBB was found to bind to NDUFAF5, which is an important subunit of CI (Figure 4A). NDUFAF5 is involved in the early-stage assembly of the CI and is closely related to protein translation of the mitochondrial gene ND1 and mitochondrial activity (Carilla-Latorre et al., 2013). However, the interaction and regulation between HBB and NDUFAF5 remain unclear. Therefore, co-immunoprecipitation (Co-IP) experiments were performed to confirm this binding (Figure 4B). RT-qPCR was performed to determine the regulation of NDUFAF5 by lncRNA16. The results revealed almost no difference in NDUFAF5 mRNA levels between A549 and A549/DDP cells (Figure S9A in Supporting Information). In addition, lncRNA16 had almost no effect on the NDUFAF5 mRNA levels (Figure S9B and C in Supporting Information). Western blot analysis showed that NDUFAF5 protein levels were upregulated in A549/DDP cells, and the protein levels of NDUFAF5 were regulated by lncRNA16 (Figure 4C). Rescue experiments suggested that lncRNA16 knockdown reduced NDUFAF5 expression, which was reversed by HBB overexpression (Figure 4D). In addition, HBB knockdown inhibited the upregulation of NDUFAF5 caused by lncRNA16 overexpression (Figure 4E), confirming that lncRNA16 regulates NDUFAF5 via HBB. HBB had little effect on the transcription of NDUFAF5 (Figure S9D and E in Supporting Information). In contrast, western blotting revealed that HBB contributed to NDUFAF5 expression (Figure 4F). An effect at the translational or post-translational level is likely responsible, which has been proven by the fact that the upregulated NDUFAF5 protein had similar mRNA levels in the HBB-overexpressing group compared to the control group. Thus, we propose that HBB facilitates the stability of NDUFAF5 and promotes its degradation. Considering that the ubiquitin-proteasome system is the main pathway of protein degradation (Paudel et al., 2023), we knocked down HBB and detected NDUFAF5 protein in the presence of cycloheximide, a protein synthesis inhibitor, and found a significantly decreased protein level of NDUFAF5 in the HBB knockdown group (Figure 4G). As expected, HBB knockdown significantly increased the ubiquitination of NDUFAF5 (Figure 4H), indicating that HBB binds to NDUFAF5 and contributes to NDUFAF5 upregulation via the ubiquitin-proteasome pathway. Previous studies have shown that a lack of NDUFAF5 resulting from RNA interference (RNAi) knockdown significantly reduces the steady state and activity of mitochondrial complex I (Sugiana et al., 2008; Yang et al., 2021). Therefore, we investigated whether HBB regulates CI activity via NDUFAF5. As was shown in Figure S10A–D in Supporting Information, HBB/NDUFAF5 knockdown or overexpression resulted in a corresponding decrease or increase in CI activity, respectively (Figure S10A–D in Supporting Information). Additionally, we demonstrated that NDUFAF5 inhibits ROS levels by measuring ROS levels upon NDUFAF5 knockdown or overexpression (Figure S10E and F in Supporting Information). Combining the above results with the fact that HBB inhibited ROS levels (Figure 3D and E), we demonstrated that HBB and NDUFAF5 facilitate the homeostasis and activity of complex I. In addition, our study suggests that HBB binds to NDUFAF5 and promotes an increase in NDUFAF5 protein levels by inhibiting its degradation via the ubiquitination pathway (Figure 4B, F and H). Taken together, we concluded that HBB bound to NDUFAF5 and stabilized its protein, thereby contributing to the maintenance of homeostasis and the activity of complex I. Together, lncRNA16 regulated the HBB/NDUFAF5 axis, substantially decreasing ROS levels.

LncRNAs can act as scaffolds to facilitate protein interactions (Tsai et al., 2010). Hence, lncRNA16 was knocked down to examine its effects on the binding of HBB to NDUFAF5. A weak interaction was observed between HBB and NDUFAF5 (Figure 4I). In contrast, lncRNA16 overexpression substantially enhanced their binding (Figure 4I). To investigate whether the weakened interaction between HBB and NDUFAF5 was caused by lncRNA16 knockdown, we transfected HBB overexpression vectors or empty vectors upon knocking down lncRNA16 and then evaluated the binding of HBB and NDUFAF5 by Co-IP analysis. Although overexpression of HBB increased the protein levels of HBB and NDUFAF5, the binding between HBB and NDUFAF5 was attenuated when lncRNA16 was knocked down (Figure 4J). The interaction between HBB and NDUFAF5 was also attenuated when RNase was added to degrade the RNA (Figure 4K). Thus, lncRNA16 acts as a scaffold to facilitate the binding of HBB and NDUFAF5.

LncRNA16 facilitates the colocalization of HBB and NDUFAF5 in the mitochondria

To investigate the role of lncRNA16 in the colocalization of HBB and NDUFAF5, the locations of lncRNA16, HBB, and NDUFAF5 were investigated. The results showed that lncRNA16, HBB, and NDUFAF5 were located in the mitochondria (Figure 5A; Figure S7B–D in Supporting Information) and that lncRNA16, HBB, and NDUFAF5 were colocalized in the mitochondria (Figure 5B; Figure S7E in Supporting Information). Western blotting showed that lncRNA16 promoted the accumulation of HBB and NDUFAF5 in the mitochondria (Figure 5C), which was also verified by IF analyses (Figure 5D and E), indicating that lncRNA16 was essential for the colocalization of HBB and NDUFAF5 in the mitochondria.

NDUFAF5 facilitates chemoresistance

Based on these results, we evaluated the effects of NDUFAF5 on DDP resistance. MTS experiments revealed that when NDUFAF5 was knocked down, the presence of DDP significantly attenuated the viability of A549/DDP cells (Figure 6A). Moreover, NDUFAF5 knockdown significantly inhibited cell proliferation compared to the control group treated with DDP (Figure 6A). In contrast, NDUFAF5 overexpression facilitated cell proliferation regardless of the presence of DDP in A549 cells (Figure 6B). Additionally, colony formation assays further validated these results (Figure 6C–F), corroborating the finding that NDUFAF5 improved DDP resistance. To further understand the role of NDUFAF5 in clinical chemoresistance, 34 NSCLC patients in the TCGA dataset were analyzed. The results revealed that NDUFAF5 mRNA levels were higher at baseline in non-responsive patients than in responsive patients (Figure 6G), whereas in the results of immunohistochemical analyses of pre-treatment NSCLC tissues from 47 patients, the responders and non-responders showed almost the same NDUFAF5 protein levels (Figure 6H). Interestingly, after receiving platinum-based treatment, NDUFAF5 protein levels in the response group significantly decreased, whereas the non-response group showed the opposite results, which caused more significant post-treatment differences between the two groups

https://doi.org/10.1007/s11427-023-2434-8

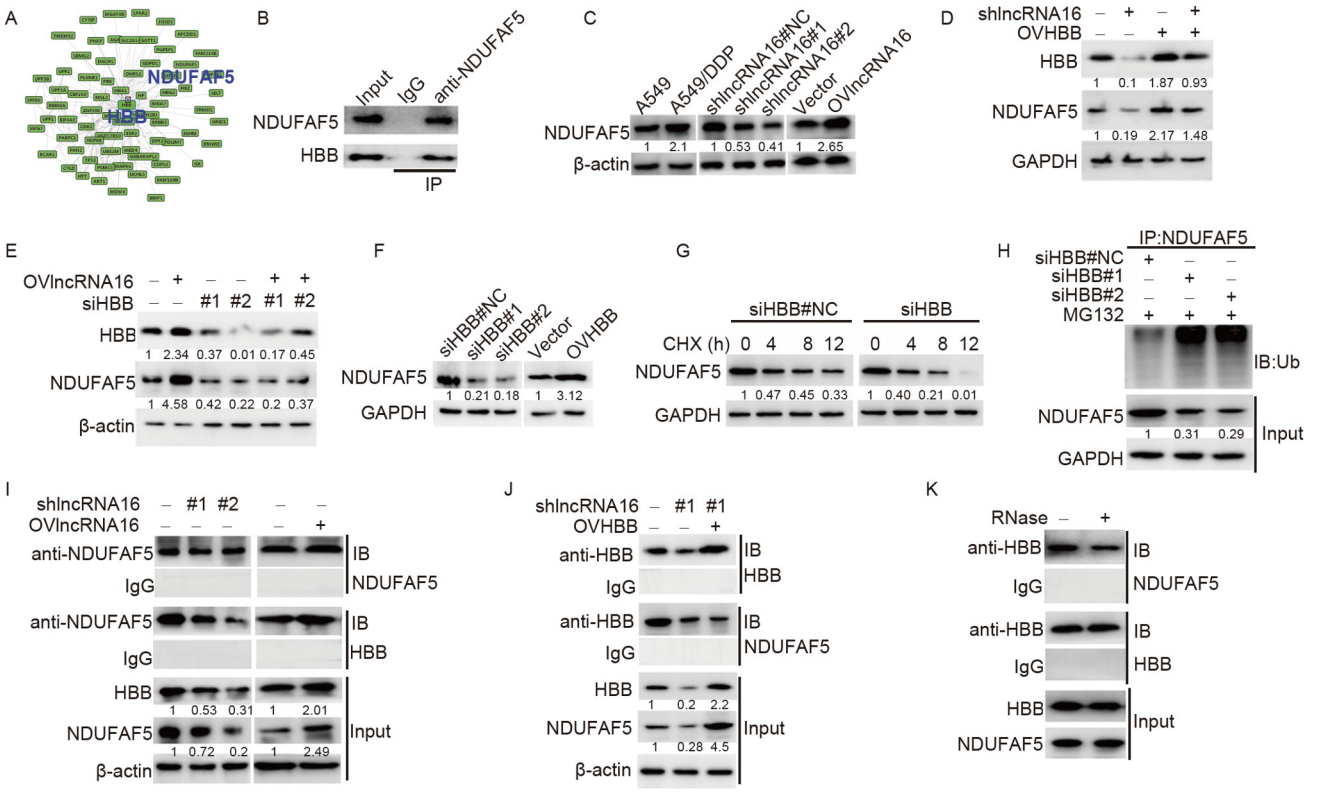

Figure 4. LncRNA16 acts as a scaffold to facilitate the binding of HBB and NDUFAF5. A, Analysis of HBB-binding proteins by online tools (http://gpsprot.org/). B, Co-IP analyses were performed to confirm the binding of HBB with NDUFAF5. C, Western blots were performed to investigate the effects of lncRNA16 on NDUFAF5 protein levels. D–E, A rescue assay was performed to confirm that lncRNA16 regulated NDUFAF5 via HBB. F, Western blots were performed to investigate the effects of HBB on NDUFAF5 protein levels. G, Western blots were performed to investigate the effects of HBB knockdown on the expression of NDUFAF5 protein in the presence of CHX. H, Ubiquitinated NDUFAF5 was detected by immunoprecipitation with anti-NDUFAF5 antibody in A549/DDP cells transfected with NC or HBB-siRNAs. I, Co-IP was performed to investigate the effects of lncRNA16 on the binding of HBB with NDUFAF5. J, Co-IP was performed to investigate the effects of lncRNA16 knockdown combined with HBB overexpression on the binding of HBB with NDUFAF5. K, Co-IP was performed to investigate the effects of RNase treatment on the binding of HBB with NDUFAF5.

(Figure 6H), indicating that NDUFAF5 contributes to chemoresistance.

Intervention of lncRNA16 with siRNA inhibits tumor progression *in vitro* and *vivo*

Targeting lncRNA16 is a promising strategy for overcoming chemoresistance. RNAi therapy has received widespread attention and achieved significant breakthroughs in preclinical models by targeting specific genes, enabling precise and personalized treatment with high safety and lasting effects (Davis et al., 2010; Elbashir et al., 2001; Li et al., 2020); therefore, two siRNAs were designed to target lncRNA16, with knockdown efficiencies of 40% and 60%, respectively (Figure 7A). MTS experiments suggested that these two siRNAs significantly retarded cell proliferation (Figure 7B). Nevertheless, the inhibitory effects on colony formation were observed only in the silncRNA16#2 group (Figure 7C). Thus, silncRNA16#2 was selected for follow-up studies. It's well known that siRNA was easily degraded by nucleases *in vivo* (Ambardekar et al., 2011). SilncRNA16#2 was modified with cholesterol for stabilization to avoid degradation and increase the persistence of RNAi *in vivo* and labeled with cy3 fluorescence for visualization. Confocal imaging illustrated successful cellular uptake of silncRNA16#2 by A549/DDP cells 4 h after transfection (Figure 7D). Importantly, modified silncRNA16#2 (named cy3-silncRNA16#2) exerted substantial knockdown efficiency of lncRNA16, inhibited the HBB/NDUFAF5 axis, accelerated ROS generation, and caused significant retardation of cell proliferation (Figure 7E–H). Overall, the chemical modification did not impair the inhibitory effects of silncRNA16#2 on cell proliferation.

To further explore the chemoresistance-overcoming effects of lncRNA16 interference *in vivo*, A549/DDP-bearing mouse models were established, and cy3-siRNA and DDP were administered every three days for a total of four cycles (Figure 7I). After all treatments, the mice were sacrificed, and the tumors in the groups are shown in Figure 7J. Notably, the administration of DDP in combination with cy3-silncRNA16#2 significantly inhibited tumor growth without a loss of body weight (Figure 7J; Figure S11A and B in Supporting Information). Hematoxylin and eosin (H&E) staining revealed no structural abnormalities in the livers or kidneys (Figure 7K). Taken together, targeting lncRNA16 leads to safe and effective growth retardation of tumors.

Nano-based delivery of siRNA exhibits more significant tumor suppression effects than siRNA

Nanocarriers are widely used for RNAi delivery because they efficiently mediate RNAi (Zou et al., 2020). Because of their highly effective delivery potential, GalNAc-conjugated RNAi drugs currently account for one-third of RNAi drugs in clinical

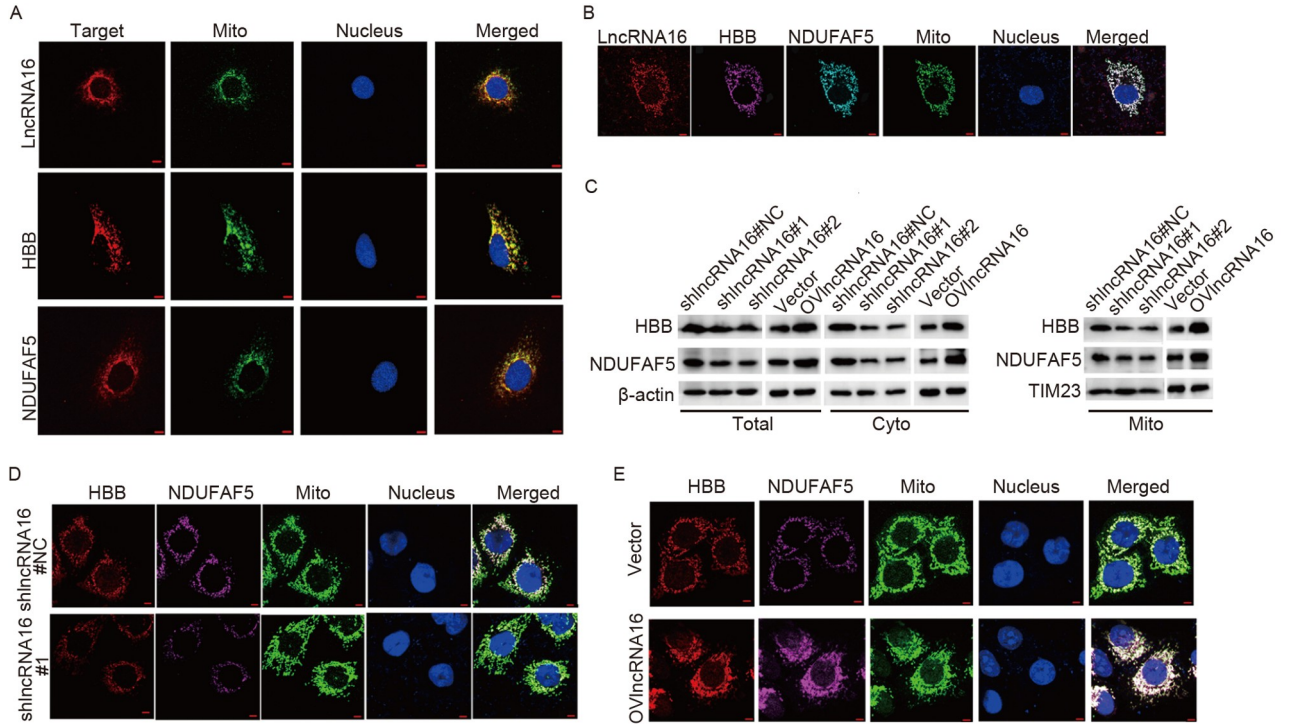

Figure 5. LncRNA16 facilitates the colocalization of HBB and NDUFAF5 in the mitochondria. A, FISH and IF assays were performed to show the location of lncRNA16, HBB, and NDUFAF5 in the mitochondria. B, FISH and IF assays were combined to show the colocalization of lncRNA16, HBB, and NDUFAF5 in the mitochondria. C, Western blots were performed to investigate the effects of lncRNA16 on the accumulation of HBB and NDUFAF5 in the mitochondria. β-actin and Tim23 were used as cytoplasmic and mitochondrial references, respectively. D, IF assay was performed to investigate the effects of lncRNA16 knockdown on the accumulation of HBB and NDUFAF5 in the mitochondria. E, IF assay was performed to investigate the effects of lncRNA16 overexpression on the accumulation of HBB and NDUFAF5 in the mitochondria. Scale bars represented 5 μm.

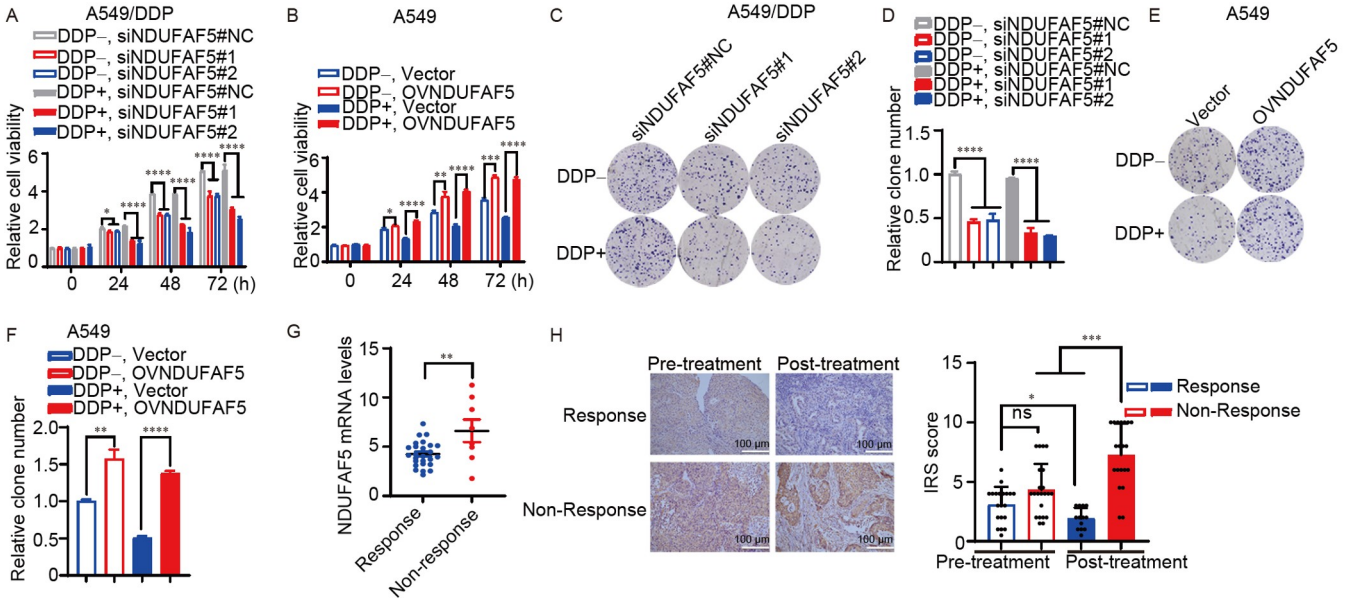

Figure 6. NDUFAF5 facilitates chemoresistance. A and B, MTS assay was performed to investigate the effects of NDUFAF5 on cell viability. C–F, Colony formation assays were performed to investigate the effects of NDUFAF5 on cell proliferation. G, Comparison of pre-treatment NDUFAF5 mRNA levels among the response (n=26) and non-response (n=8) NSCLC patients in TCGA datasets. H, IHC analyses were performed to detect pre- and post-treatment NDUFAF5 protein changes among 47 NSCLC patients. For A and B, statistical significance was calculated with two-way ANOVA. For C–F, statistical significance was calculated with one-way ANOVA. For G and H, statistical significance was calculated with the Mann-Whitney U-test. *, P<0.05; **, P<0.01; ***, P<0.001; ****, P<0.0001; ns, non-significance.

trials (Kanasty et al., 2013). GIVLAARI, the first marketed RNAi therapy, was also developed based on GalNAc delivery, suggesting it is safe for clinical applications (Huang et al., 2022). GalNAc is a natural ligand of the asialoglycoprotein receptor (ASGPR), which is highly expressed in hepatocytes and also expressed in extrahepatic cancer cells such as A549, MCF7, and HCT116,

https://doi.org/10.1007/s11427-023-2434-8

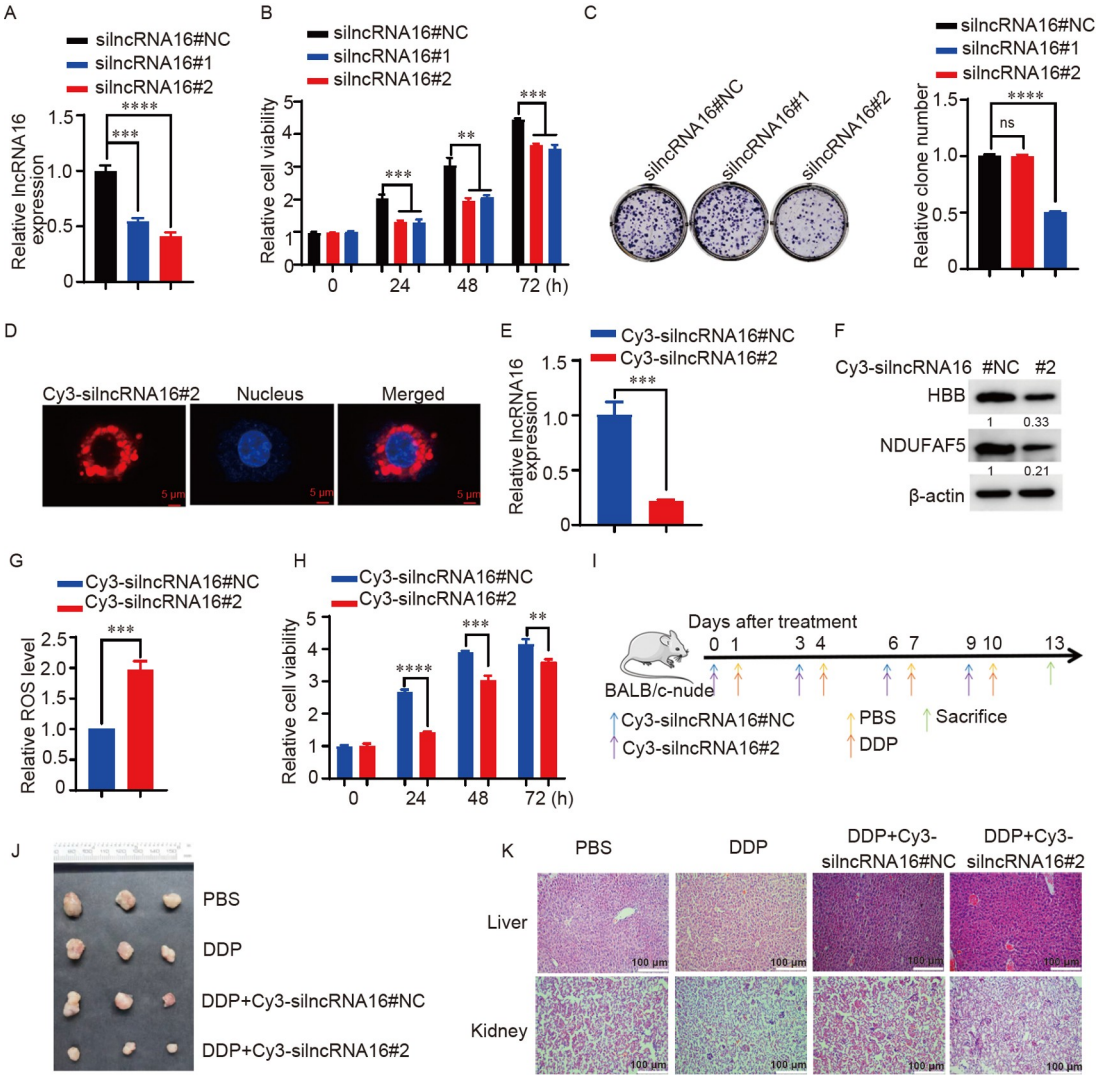

Figure 7. LncRNA16 interference inhibits tumor progression *in vitro* and *in vivo*. A, RT-qPCR was performed to investigate whether siRNA could efficiently knock down lncRNA16; B, MTS assays were performed to detect cell inhibition after lncRNA16 interference by siRNA. C, Colony formation assays detected cell proliferation after lncRNA16 intervention by siRNA. D, The uptake of cy3-silncRNA16#2 by A549/DDP cells was observed using confocal microscope 4 h after transfection. E, RT-qPCR was performed to detect the knockdown efficiency of lncRNA16 by chemically modified siRNA (cy3-silncRNA16#2). F, Western blotting was performed to detect the effects of modified siRNA on the HBB/NDUFAF5 axis. G, Flow cytometry analysis was performed to investigate the effects of modified siRNA on ROS levels. H, MTS assays were performed to detect cell proliferation by chemically modified siRNA. I, Construction of subcutaneous xenograft models and the frequency of therapy administration. The A549/DDP-bearing mice were administered with cy3-silncRNA16 (subcutaneously, 0.5 mg kg^{-1}) or/and DDP (intraperitoneally, 5 mg kg^{-1}) every three days for four cycles. cy3-silncRNA16#NC was used as the negative control of cy3-silncRNA16#2, and PBS was used as the negative control of DDP. J, Picture of tumors among groups. K, H&E staining was performed to observe structure abnormalities in the livers and kidneys. For A and C, statistical significance was calculated with one-way ANOVA. For B and H, statistical significance was calculated with two-way ANOVA. *, $P<0.05$; **, $P<0.01$; ***, $P<0.001$; ****, $P<0.0001$; ns, non-significance.

representing a broad ligand for multiple tumor imaging and therapy (Ma et al., 2015; Nair et al., 2017; Sun et al., 2020). Therefore, GalNAc conjugates are not only applied in treating liver disease, but also in lung, pancreas, and colorectal cancer in phase II or III clinical trials (Winkle et al., 2021). These results indicated the potential application of GalNAc conjugates in extrahepatic diseases. The abundance of lncRNA16 in tumors and higher lncRNA16 levels in chemo-resistant tumors make it possible to target lncRNA16 based on GalNAc delivery in extrahepatic tumors. Importantly, this treatment integrates the advantages of GalNAc with convenient administration, stable metabolism, and non-toxic side effects (Brown et al., 2020; Yu et al., 2021). Therefore, GalNAc-conjugated lncRNA16 intervention provides a novel strategy for tumor targeting and efficient cancer inhibition.

GalNAc-silncRNA16 (named Nano-silncRNA16) was prepared as shown in Figure S12A in Supporting Information. The 5′ sense strand of Nano-silncRNA16 was attached to cholesterol, and the antisense strand was synthesized with cy3 linked. After the construction, mass spectrometry detection showed that the molecular weight of Nano-silncRNA16 was 7,337.075 D, with a small deviation of −0.053% compared with the standard weight, demonstrating the successful construction of Nano-silncRNA16 (Figure S12B in Supporting Information). Subsequently, the shape of Nano-silncRNA16 was observed using transmission electron microscopy (TEM), which revealed that Nano-silncRNA16 was spherical with an average size of 26.57 nm (Figure S12C and D in Supporting Information).

Moreover, Nano-silncRNA16 was successfully taken up by A549/DDP cells 6 h after transfection (Figure 8A). To compare the inhibition effects of silncRNA16 and Nano-silncRNA16 on lncRNA16, RT-qPCR was performed. The results showed that Nano-silncRNA16 exerted a higher lncRNA16 knockdown efficiency than silncRNA16, with a rate of 85.7% *vs.* 78.5% (Figure 8B). Moreover, more potent inhibition of cell proliferation was produced by Nano-silncRNA16 (Figure 8C), indicating that GalNAc delivery substantially enhanced RNAi function. To compare the anti-chemoresistance effects of silncRNA16 and Nano-silncRNA16 *in vivo*, A549/DDP-bearing mice were randomly divided into five groups, and six cycles of lncRNA interference with DDP or phosphate buffer solution (PBS) were administered as follows: siRNA or Nano-siRNA was injected subcutaneously on day 1, and PBS or DDP was administered intraperitoneally on day 2 (Figure 8D). Fluorescence intensity was analyzed to compare the enrichment of silncRNA16 and Nano-silncRNA16 in the tumors and organs. The results showed that the fluorescence intensity was high in the tumor, liver, and kidney but relatively weak in the lung, spleen, and heart (Figure 8E). Moreover, the fluorescence enrichment of Nano-silncRNA16 in tumors was significantly higher than that of silncRNA16 at 0.5 and 2 h (Figure 8E), illustrating that GalNAc delivery effectively increased the accumulation and retention of silncRNA16 in tumors. After completing all administration cycles, the mice were sacrificed, and the tumors among the groups are shown in Figure 8F. The combination of DDP and silncRNA16 effectively hampered tumor growth. Notably, Nano-silncRNA16 exerted higher tumor suppression effects than silncRNA16 (Figure 8F and G) without weight loss or organ damage (Figure 8H; Figure S13 in Supporting Information). Moreover, histopathological evaluation by H&E staining showed that Nano-silncRNA16 did not cause any significant changes in organ morphology (Figure 8I). Considering that systemic toxicity has always been a critical concern when using nanodrugs *in vivo*, we collected plasma samples and performed biochemical functional analysis. Notably, no statistical differences were found in total protein (TP), albumin (ALB), aspartate aminotransferase (AST), alkaline phosphatase (ALP), and glutamyltransferase (GGT) levels among the groups (Figure S14A, B, and D–F in Supporting Information). In addition, apparent differences in alanine aminotransferase (ALT) and direct bilirubin (DBIL) were observed in the silncRNA16 combined with the DDP group but not in the Nano-silncRNA16 combined with the DDP group, revealing that GalNAc possessed superior advantages in decreasing *in vivo* toxicity (Figure S14C and G in Supporting Information). In addition, renal function and myocardial enzyme analyses showed almost no differences between the groups (Figures S15 and S16 in Supporting Information). Taken together, Nano-silncRNA16 exerted more significant tumor suppressive effects than silncRNA16.

DISCUSSION

As newly discovered functional ncRNAs, lncRNAs exert extensive effects through multiple mechanisms. Recently, lncRNAs have been reported to regulate mitochondrial function, ROS generation, and cellular dysfunction (Zhang et al., 2022b; Zhang et al., 2022c; Zhang et al., 2022d). LncRNA DLEU2 regulates the activity of mitochondrial complexes and inhibits ROS generation through an intermediate protein (Zhang et al., 2022c). LncRNA PELATON and p53 can form a complex through the RBP EIF4A3, which affects mitochondrial function and ROS accumulation (Fu et al., 2022). In this study, we demonstrated that lncRNA16 facilitates the binding of HBB and NDUFAF5 in the mitochondria, thereby enhancing complex I activity, suppressing ROS generation, and eventually promoting chemoresistance in NSCLC.

RNA pull-down and nucleotide-protein docking analyses indicated that lncRNA16 bound tightly to HBB through truncations T1, T2, and T4, with an extremely low binding energy of $-1{,}194.646$ kcal mol^{-1} and according to the results of nucleotide-protein docking, T1, T2, and T4 formed hydrogen bonds and salt bridges with HBB. In addition, T4 formed two π-π bonds with HBB, contributing to the binding stability between lncRNA16 and HBB. We demonstrated that lncRNA16 promotes HBB protein upregulation by inhibiting autophagy. However, the mechanisms by which lncRNA16 regulates autophagy and whether the binding of lncRNA16 to HBB affects autophagy remain unknown and need to be determined in further studies.

HBB is an essential oxygen carrier and regulates ROS production (Zheng et al., 2017). Proteins in the mitochondria usually contain an N-terminal leader peptide, which is critical for their import into the mitochondria (Arena et al., 2018). However, the HBB protein sequence analysis failed to detect mitochondrial localization signals. NDUFAF5, located in the matrix of the mitochondrial inner membrane, is a critical subunit of the electron transport chain (ETC) complex I (Fiedorczuk and Sazanov, 2018). Therefore, we speculated that the import of HBB into the mitochondria depended on NDUFAF5. As expected, NDUFAF5 knockdown did not affect the total expression of HBB but decreased HBB protein in the mitochondria (Figure S17A in Supporting Information), indicating an important role of NDUFAF5 in the mitochondrial import of HBB. Additionally, we analyzed the potential binding mode of NDUFAF5 to HBB using a protein docking study (Figure S17B in Supporting Information). The results revealed that the 210–270 amino acid (aa) of NDUFAF5 and HBB formed a protein interaction interface. Specifically, GLY-210, ASN-269, ALA-221, and ASN-223 of NDUFAF5 formed hydrogen bonds with HBB, stabilizing NDUFAF5-HBB complexes. To further confirm that the interaction between the two was critical for the entry of HBB into the mitochondria, FLAG-tagged truncated mutants of NDUFAF5 with deletions of 210–270 aa were constructed. Co-IP assays of the mitochondrial lysates indicated that wild-type NDUFAF5 interacted with HBB, whereas the truncated mutants did not (Figure S17C in Supporting Information), indicating the necessity of 210–270 aa of NDUFAF5 for the mitochondrial import of HBB. As a mitochondria-located protein, the transport of NDUFAF5 requires the assistance of translocation systems such as the TOM and TIM23 complexes (Paschen and Neupert, 2001). Therefore, to further determine the mitochondrial import of HBB and NDUFAF5, additional experiments should be designed to determine whether the import of HBB and NDUFAF5 requires the help of translocation systems. In addition, to explore whether the interaction between HBB and NDUFAF5 is critical for the mitochondrial import of HBB, designing inhibitory peptides using Peptiderive server to block their interactions specifically seems better (Yang et al., 2021), as this method maintains the standard structure of NDUFAF5. However, we did not choose this solution because of time constraints.

In this study, we demonstrated that HBB facilitated the

https://doi.org/10.1007/s11427-023-2434-8

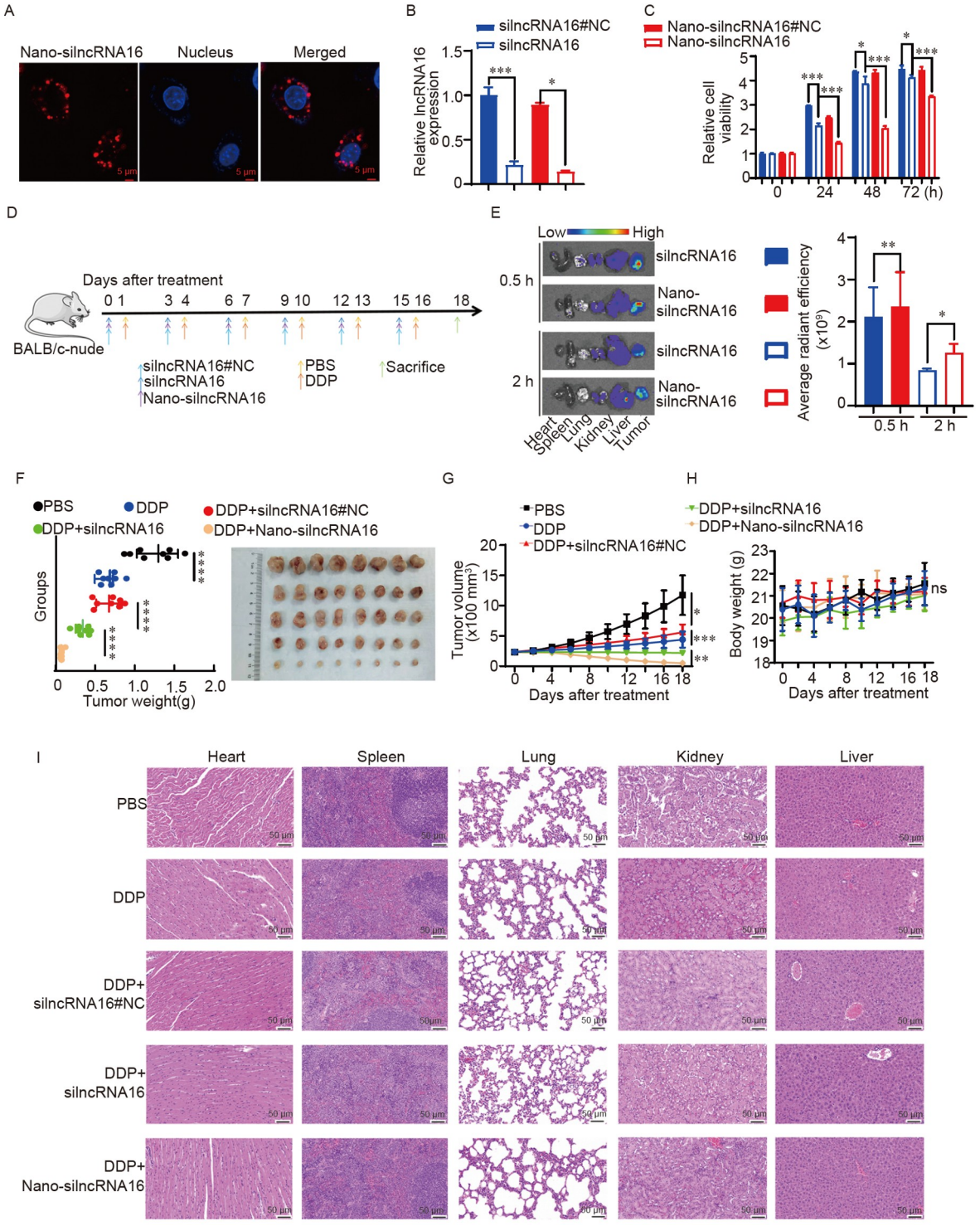

Figure 8. The comparison of tumor inhibition effects by silncRNA16 and Nano-silncRNA16. A, Cellular uptake of Nano-silncRNA16 by A549/DDP cells was examined under a confocal microscope 6 h after Nano-silncRNA16 transfection. B, RT-qPCR was performed to compare the knockdown efficiency of lncRNA16 by silncRNA16 and Nano-silncRNA16. C, MTS assays were performed to compare cell inhibition by silncRNA16 and Nano-silncRNA16. D, The construction of subcutaneous xenograft models and the frequency of therapy administration. E, Fluorescence imaging was performed to compare the enrichment of silncRNA16 and Nano-silncRNA16 in tumors after administration at 0.5 and 2 h, n=3 per group. F and G, Pictures of tumors, tumor weight, and tumor volumes among groups. H, The curve of body weight. I, H&E staining was performed to observe structure abnormalities in organs. For B, E–H, statistical significance was calculated with one-way ANOVA. For C, statistical significance was calculated with two-way ANOVA. *, P<0.05; **, P<0.01; ***, P<0.001; ****, P<0.0001; ns, non-significance.

upregulation of NDUFAF5 protein levels by inhibiting its degradation via the ubiquitin-proteasome pathway. However, the mechanism underlying this phenomenon remains unknown and must be elucidated. We predicted the potential protein binding with NDUFAF5 using online tools (http://gpsprot.org/) and found potential binding between the E3 ubiquitin ligase

DTX3 and NDUFAF5 (Figure S18A in Supporting Information). As stated in a previous report, DTX3 contains a classic RING finger domain that facilitates the ubiquitination and degradation of target proteins by binding to them (Ding et al., 2020). In addition, protein-protein docking was performed to simulate the spatial binding between DTX3 and NDUFAF5. These results indicate a stable binding between them, with a low binding energy of −1,125.881 kcal mol^{-1}. Specifically, GLU-253, GLU-256, and ARG-276 in NDUFAF5 formed hydrogen bonds with DTX3 (Figure S18B in Supporting Information). Remarkably, our predictions showed that GLU-253 and GLU-256 were included in the 210–270 aa of NDUFAF5, the interaction interface between NDUFAF5 and HBB, indicating the possibility of competitive binding of HBB and DTX3 with NDUFAF5. We speculated that when HBB was knocked down, the decrease in HBB protein levels might have contributed to the increased binding between DTX3 and NDUFAF5, which might have promoted the degradation of NDUFAF5. This is an interesting topic worthy of further research.

Mitochondrial oxidative respiration is essential for tumor growth (Yang et al., 2021). NDUFAF5, a key component of mitochondrial complex I, is crucial for its stability and activity. In this study, we demonstrated that lncRNA16 promotes the binding of HBB to NDUFAF5, further inhibiting the degradation of NDUFAF5, thereby leading to an increase in complex I activity and providing a new mechanism for regulating mitochondrial activity.

Precise cancer therapy can prolong patients' life. Targeting chemoresistance-promoting genes is a promising strategy in cancer therapy (Li et al., 2022; Stine et al., 2022). RNAi has the potential for cancer therapy because of its precise, personalized, safe, lasting, and effective treatment (Davis et al., 2010; Zhang and Zhang, 2023). Among all RNAi therapies in clinical trials, STP705, consisting of two siRNA oligonucleotides targeting TGF-β1 and COX-2, is the most concerned and has shown positive efficacy in a phase IIa clinical trial in situ squamous cell carcinoma, with 66.6667% (10/15) of patients achieving complete histological clearance of tumor tissues without adverse effects related to the treatment (Sirnaomics, Inc, 2020), indicating the superior potential of RNAi therapy and the necessity of developing effective RNAi targets. The number of ncRNAs far exceeds that of protein-coding genes (Aguilar et al., 2022); moreover, lncRNAs have multiple functions and are widely distributed in human tissues. Therefore, lncRNAs rapidly become novel potential biomarkers and therapeutic targets, opening a wide field for developing new drugs against diseases (Patil et al., 2016). An increasing number of studies have indicated a critical role of lncRNAs in chemoresistance (Shi et al., 2020), demonstrating that lncRNA intervention is a direct and effective way to promote chemosensitivity. To date, 11 RNA-based drugs that target mRNAs or pre-mRNAs have been approved by the FDA or EMA (Winkle et al., 2021). However, the development and application of lncRNA-targeted therapies are limited. LncRNA interventions have great potential for cancer inhibition. Antisense nucleotides (ASO) drugs for targeting lncRNA have shown promising results in preclinical and clinical trials (Gong et al., 2019; Pan et al., 2023; Viney et al., 2016). LncRNA16 is highly expressed in tumors, especially in chemo-resistant cancers; therefore, lncRNA16 targeting is promising for effective cancer therapy.

Nanotechnology also has potential applications in biomedicine. Nanocarriers can also mediate effective RNAi for the delivery of nucleic acid-based therapeutics and have attracted extensive attention from researchers (Pan et al., 2023; Qi et al., 2021). GalNAc is clinically advanced, conveniently administered, and stably metabolized, making it widely applicable in RNAi delivery for cancer therapy (Brown et al., 2020; Yu et al., 2021). The natural receptor of GalNAc is highly expressed in hepatocytes (Nair et al., 2017), which makes GalNAc-based therapeutics widely applicable to liver diseases. However, studies have shown that GalNAc is also a broad ligand for extrahepatic tumors, such as breast, lung, and colon cancer (Ma et al., 2015; Sun et al., 2020). In phase II or III clinical trials, investigators have used GalNAc conjugates to treat extrahepatic cancers, such as lung, pancreas, and colorectal cancers (Winkle et al., 2021). GalNAc promotes the internalization of chemotherapeutic drugs into cancer cells (Aviñó et al., 2021). Although GalNAc contributes to the internalization of 5-fluorouracil in the hepatoma cell line HepG2 owing to the high expression of ASGPR, the internalization efficiency in HepG2 cells (39%) was still lower than that in extrahepatic cancer cell lines, such as HTB-38 (87%) and HCC2998 (70%) (Aviñó et al., 2021). In addition, cancer cells with high or low ASGPR expression showed similar uptake rates of GalNAc conjugates when exposed to a specific concentration range (Petrov et al., 2021). These results indicate the existence of other cellular uptakes of GalNAc conjugates and the potential application of GalNAc conjugates even in extrahepatic diseases with low ASGPR levels. In this study, high levels of lncRNA16 in tumors were critical for successful lncRNA16 targeting. In addition, the stability of silncRNA16 mediated by GalNAc, enhanced permeability and retention effects of GalNAc conjugates, and multiple endocytosis mechanisms in cells are important for promoting anti-tumor efficacy. Therefore, GalNAc-conjugated silncRNA16 has advantages for the treatment of chemo-resistant cancers. Therefore, it is important to explore the extrahepatic applications of GalNAc conjugates.

We reported an increased abundance of lncRNA16 in the serum of patients with platinum resistance and provided evidence that it might serve as a valuable diagnostic marker for distinguishing chemoresistant patients. Mechanistically, we demonstrated that lncRNA16 promoted the binding of HBB and NDUFAF5 in the mitochondria, and the lncRNA16/HBB/NDUFAF5 axis was identified as a novel pathway that regulates mitochondrial ROS generation. Nano-silncRNA16 notably enhanced the intervention efficiency of lncRNA16 and significantly attenuated chemoresistance by promoting ROS generation (Figure 9). Notably, Nano-silncRNA16 achieved tumor growth retardation *in vivo* without causing systemic toxicity, making it a promising therapeutic strategy for clinical applications.

LncRNA16 inhibits ROS generation in chemo-resistant cells, indicating its importance as a promising target for resisting ROS-driven chemoresistance. Wang et al. (2019) reported a novel pH/ROS dual-responsive nanoparticle that contributed to doxorubicin release through ROS-induced thioketal bond breaking to realize a cascade of ROS generation and enhanced anti-tumor efficacy. Zheng et al. (2019) constructed a unique nano-drug with a potent siRNA release triggered by tumor-derived ROS that exhibited excellent blood-brain barrier penetration and significantly enhanced treatment efficacy in glioblastoma. In this study, if ROS induction and lncRNA16 intervention are combined, stronger anti-tumor effects might be observed.

In conclusion, Nano-silncRNA16 caused pronounced tumor

https://doi.org/10.1007/s11427-023-2434-8

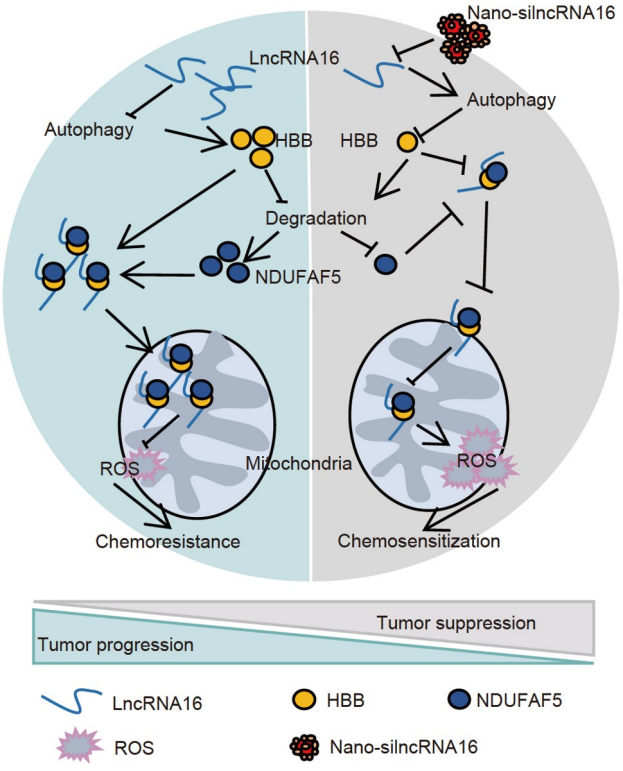

Figure 9. Schematic diagram of lncRNA16 promoting chemoresistance and chemotherapeutic sensibilization exerted by lncRNA16 intervention via Nano-silncRNA16 LncRNA16 is highly expressed in chemo-resistant cancer cells, contributes to chemoresistance through ROS inhibition via the novel HBB/NDUFAF5 axis, and functions as a scaffold to facilitate the colocalization of HBB and NDUFAF5 in the mitochondria. LncRNA16 intervention by Nano-silncRNA16 significantly improves chemosensitivity and contributes to tumor suppression.

growth retardation and remarkably restored chemosensitivity *in vitro* and *in vivo*, illustrating the potential clinical application of Nano-silncRNA16 in anti-chemoresistance.

MATERIALS AND METHODS

Patient samples

Pre-treatment plasma samples from 35 NSCLC patients, paired pre- and post-treatment serum samples from 10 NSCLC patients, and 188 tissue specimens from 47 NSCLC patients were obtained from the Peking University Cancer Hospital. After the collection of pre-treatment samples, these patients received only platinum-based chemotherapy. Pre- and post-treatment tissue samples were collected via endoscopic biopsy and surgery, respectively. The expression of HBB and NDUFAF5 was detected using IHC assays. Post-treatment tissues without tumor areas confirmed by IHC assays were excluded from the analyses. Finally, 84 pre- and 66 post-treatment tumor samples were analyzed. Patient prognoses were evaluated according to the Response Evaluation Criteria for Solid Tumors (RECIST). Response patients indicated chemo-sensitivity and non-response patients indicated chemo-resistance. Response and non-response were defined as follows: complete response (CR) and partial response (PR) belonged to the response group, and progressive disease (PD) and stable disease (SD) belonged to the non-response group. This study was approved by the Ethics Committee of the Peking University Cancer Hospital and Institute (2020KT50). The sequencing data of patients with NSCLC were downloaded from TCGA database (https://cancergenome.nih.gov). The sequencing data were transformed into transcripts per kilobase million (TPM) and used for expression analyses of HBB and NDUFAF5. A total of 34 patients who underwent neoadjuvant platinum-based chemotherapy with a clear efficacy evaluation were included in the analyses.

Cell lines

The NSCLC cell lines used in this study were A549, H460, H226, H520, PC-9, and SK-MES-1. The corresponding DDP-resistant cell lines were named as A549/DDP, H460/DDP, H226/DDP, H520/DDP, PC-9/DDP, and SK-MES-1/DDP. Except for A549/DDP, all other cell lines were purchased from Qing Qi (Shanghai) Biotechnology Development Co., Ltd (Shanghai, China). The A549/DDP cells were established in the laboratory. Parental A549 cells were treated with cisplatin (DDP) 0.2 μg mL^{-1} (Selleck, USA). Subsequently, the concentrations were gradually increased to 2 μg mL^{-1} over six months, and the surviving cells were maintained at 1 μg mL^{-1} of DDP. A549 and A549/DDP cells were cultured in Dulbecco's Modified Eagle's Medium (DMEM) (GIBCO, Thermo Fisher Scientific, USA) containing 10% fetal bovine serum (Excell Bio, Uruguay) at 37°C in a humidified atmosphere containing 5% CO_2. Cell lines were used within five generations after thawing. Short tandem repeat profiling was performed to identify the cells, and a Mycoplasma Real-time PCR Detection Kit was used to rule out mycoplasma contamination.

Cell transfection

LncRNA16 was knocked down using shRNA (Genepharma, Shanghai, China) and silncRNA16 (RiboBio, Guangzhou, China). According to the manufacturers' instructions, cells were transfected using Lipofectamine 3000 (Thermo Fisher Scientific). Detailed sequence information is provided in Table S1 in Supporting Information. Targets were efficiently knocked down (Figure S19 in Supporting Information).

Western blotting analysis and antibodies

Total protein was separated by SDS-PAGE and transferred to a 0.22 μm PVDF membrane (Merck Millipore, Germany) under constant current. The membrane was blocked with 5% skim milk at room temperature for 1 h. The primary antibody was diluted according to the instructions and incubated with the membrane overnight at 4°C. Subsequently, the membrane was incubated with a secondary antibody at room temperature for 1 h. Finally, luminescence analysis was performed using a chemiluminescence detection kit (Thermo Fisher Scientific). The antibodies used were as follows: anti-HBB (Abcam), anti-NDUFAF5 (Abcam)), anti-Tim23 (Abcam), GAPDH (CST), anti-β-actin (CST), anti-LC3 (CST), anti-P62 (CST), anti-HBA1 (Abclonal), anti-LCN1 (Abclonal).

RNA isolation and RT-qPCR

Total RNA in cells was extracted using RNAiso Plus (TaKaRa, Japan), followed by reverse transcription using a primescript™

RT reagent kit with gDNA eraser (TaKaRa). Serum RNA was extracted using the BIOG cfRNA easy kit (Baidai Biology, Changzhou, China). According to the manufacturer's instructions, real-time PCR was performed using an Applied Biosystems 7500 system. The primers used were as follows: lncRNA16 (forward: 5′-GATGACAGTCTGCCTCTATCTTAC-3′; reverse: 5′-CTTTGAGCCAAGCAGGTTATTG-3′), HBB (forward: 5′-GCACGTGGATCCTGAGAACT-3′; reverse: 5′-ACCAGCCACCACTTTCTGAT-3′), NDUFAF5 (forward: 5′-ACCTGGGACATCTGCTTGGG-3′; reverse: 5′-CTCGATGCAGCAGGGCTTTT-3′), β-actin (forward: 5′-CGAGAAGATGACCCAGATCATG-3′; reverse: 5′-GTGAAGCTGTAGCCGCGCTCGG-3′), GAPDH (forward: 5′-GGAGCGAGATCCCTCCAAAAT-3′; reverse: 5′-GCTGTTGTCATACTTCTCATGGG-3′).

FISH

FISH analysis was performed using the Ribo™ Fluorescent in Situ Hybridization Kit (RiboBio) according to the manufacturer's instructions. Cells were seeded in confocal dishes. When the cell density reached 60%–70%, the cells were fixed, permeabilized with methanol, and washed three times with PBS. Subsequently, cells were incubated with 200 μL 1× pre-hybridization buffer for 30 min at 37°C, and after that, 100 μL 1× hybridization buffer containing 2.5 μL lncRNA probe was added to incubate with the cells overnight in the dark at 37°C. The next day, the cells were washed five times with saline sodium citrate buffer for five times and then washed with PBS for one time. Finally, the cells were stained with DAPI solution for 10 min before detection.

IF

Cells were seeded in confocal dishes. When the cell density reached 80%–90%, the cells were fixed with methanol and washed with PBS for two times. Subsequently, the cells were incubated with 1% BSA solution for 30 min at 37°C. The cells were then incubated with the primary antibody for 2 h, followed by incubation with the secondary antibody for 1 h at room temperature. Finally, the cells were stained with DAPI solution for 10 min and washed with PBS three times before detection.

Colony formation assay

After digestion, 1×10^3 cells per well were seeded in six-well plates and treated for different purposes. The cell medium was removed for 10–15 d, and the cells were fixed with absolute ethanol for 15 min. Subsequently, the cells were washed with PBS three times and stained with 0.2% crystal violet for 15 min. Finally, colonies were washed under running water and photographed using a scanner. Colonies were analyzed using ImageJ 1.52a.

MTS assay

Cell viability was measured using a CellTiter 96®AQueousOne Solution Cell Proliferation (MTS) Assay (Promega, USA). Briefly, after digestion, 3×10^3 cells were seeded in 96-well plates and treated for various purposes. 48 h after, the cell medium was removed, and 100 μL DMEM medium containing 10% MTS solution was added. The cells were incubated in the dark at 37°C for 1–2 h. Finally, the cell viability was detected using an enzyme labeling instrument (Tecan Infinite M200 Pro, Tecan, Switzerland) at a wavelength of 490 nm.

ROS detection

When the cell density reached 80%–90%, the cells were washed with PBS for one time, and then 200 μL Mitosox™ Red mitochondrial superoxide indicator (Thermo Fisher Scientific) with a concentration of 5 μmol L^{-1} was added to indicate ROS levels for 10 min. Cells were washed with PBS three times and subsequently analyzed on a BD Accuri C6 flow cytometer (BD Biosciences, USA). Hoechst 33342 was used to stain the nuclei for detection via confocal microscopy, and the cells were washed with PBS three times. All staining procedures were performed in the dark.

RIP assay

According to the manufacturer's instructions, RIP assays were performed using the Magna RIP Kit (MagnaRIP01, Merck Millipore, Germany). Firstly, 5 μg μL^{-1} negative control IgG or antibody was incubated with 100 μL magnetic beads at room temperature for 1 h to prepare antibody-conjugated magnetic beads. Use lysate containing protease and RNase inhibitor to lyse cells, and then centrifuge cells at 17,000×*g* for 10 min at 4°C to obtain supernatant. Subsequently, 100 μL supernatant and the prepared magnetic bead were incubated overnight at 4°C. The mixture was centrifuged at 4,000×*g* for 2 min and washed with NT-2 buffer six times. Finally, 1 mL of TRIzol was used for RNA extraction, and RNA levels were quantified using an Applied Biosystems 7500 system.

RNA pull-down assay

The DNA templates were obtained via enzymatic digestion. The T7 High Yield RNA Transcription Kit, (Vazyme, Nanjing, China) was used for *in vitro* transcription, and the Pierce™ RNA 3′ End Desthiobiotinylation Kit (Thermo Fisher Scientific) was used to label RNA with biotin. Finally, an RNA-pull down kit (Thermo Fisher Scientific) was used to mix RNA with proteins according to the manufacturer's instructions, and the proteins were detected by Western blotting.

ChIRP-MS

The cells were harvested and lysed. Biotin-labeled probes (100 pmol L^{-1} per 2×10^7 cells) were combined with magnetic beads for 30 min, mixed with samples, and hybridized at 37°C overnight. The supernatant was obtained via enzymatic hydrolysis. The peptides were separated and analyzed using a nano-UPLC (EASY-nLC1200) coupled to a Q-Exactive mass spectrometer (Thermo Finnigan, USA). MaxQuant (Version 1.5.6.0) was used to search and quantitatively analyze the raw MS data. The protein sequence database (UniProt_organism_2016_09) was downloaded from UniProt. The peptides and proteins' false discovery rate (FDR) was controlled at 0.01.

Co-IP

Firstly, 5 μg mL^{-1} negative control IgG or anti-HBB was incubated with 100 μL magnetic beads at room temperature for 1 h to prepare antibody-conjugated magnetic beads. Subse-

https://doi.org/10.1007/s11427-023-2434-8

quently, cells were lysed and then centrifuged at 17,000×*g* for 10 min at 4°C to obtain protein supernatant. 100 μL supernatant and the prepared magnetic bead were incubated overnight at 4°C. The mixture was centrifuged at 4,000×*g* for 2 min, and the beads were washed with NT-2 buffer six times. Finally, 100 μL 1× SDS loading buffer was added, and western blotting was performed to detect the protein.

IHC staining

188 NSCLC tumor samples were fixed, deparaffinized, and rehydrated. Subsequently, the slides were soaked in 3% H_2O_2 to block the endogenous peroxidase activity. Subsequently, EDTA antigenic retrieval buffer was used to promote antigen retrieval for 8–10 min in a pressure cooker, and goat serum (ZSGB-BIO, Beijing, China) was used to block nonspecific antigens. After incubation with anti-HBB (Solarbio, Beijing, China) or anti-NDUFAF5 (Solarbio) overnight at 4°C, the slides were washed with PBS three times and subsequently incubated with universal secondary antibody (ZSGB-BIO) at room temperature for 40 min. Slides were stained with 1× DAB solution (ZSGB-BIO) and hematoxylin. The slides were then dehydrated using graded ethanol series. The immunoreactive score (IRS) was used to evaluate HBB and NDUFAF5 expression. Scores were reviewed in a double-blind manner by two experienced pathologists.

Nano-silncRNA16 preparation

Briefly, GalNAc-CPG was used as a carrier to synthesize the sense strand of Nano-silncRNA16, with cholesterol attached to the 5′ sense strand. The antisense strand was synthesized on CPG carriers, with cy3 linked. The total synthesis was performed by GenePharma. The siRNA sequences are listed in Table S1 in Supporting Information.

Cellular uptake of nanoparticles

Cells were seeded in confocal dishes (Jet Biofil, Guangzhou, China). When the cell density reached 80%–90%, 5 μL Nano-silncRNA16 was transfected with the help of a 20 μL transfect mate (GenePharma). Six hours after transfection, the cells were washed with PBS two times, and Hoechst (Beyotime Biotechnology, Shanghai, China) was used to stain the nuclei. Finally, 1 mL of complete DMEM medium was added to the cells, and the cellular uptake of the nanoparticles was detected by confocal microscopy (Leica Microsystems Heiderg GmbH, Germany).

Animal experiments

A549/DDP cells were implanted subcutaneously into four weeks old female BALB/c nude mice (Beijing Vital River Laboratory Animal Technology Co., Ltd., Beijing, China) to construct a chemo-resistant xenograft tumor model. The mice were administrated for four cycles in the experiments presented in Figure 7. During the administration of each cycle, cy3-silncRNA16#NC or cy3-silncRNA16#2 (0.5 mg kg^{-1}) was injected subcutaneously on day 1, and PBS or DDP (5 mg kg^{-1}) was administered on day 2. Mice were sacrificed after four cycles of treatment.

In vivo experiments with nano-silncRNA16 therapy, mice were grouped when the tumor size reached 200–300 mm^3. SilncRNA16 (subcutaneously, 0.5 mg kg^{-1}) or Nano-silncRNA16 (subcutaneously, 0.5 mg kg^{-1}) was administered on day 1, and DDP (intraperitoneally, 5 mg kg^{-1}) was administered on day 2 in the combination group, with a cycle of treatment every three days. All animal protocols were approved by the Animal Care and Use Committee of the Peking University Cancer Hospital & Institute (EAEC 2018-11).

In vivo biodistribution

A549/DDP tumor-bearing BALB/c nude mice were injected with Nano-silncRNA16 subcutaneously (0.5 mg kg^{-1}). The average radiant efficiencies in the major organs and tumors were measured at 0.5 and 2 h after administration using an *in vivo* imaging system (IVIS Spectrum CT, PerkinElmer). n=3 mice per group.

Statistical analysis

All statistical analyses were performed using GraphPad Prism software (version 9.0). For continuous variables that did not conform to a normal distribution, the Mann-Whitney *U*-test was used for non-paired samples, and the Wilcoxon signed-rank test was used for paired samples. For continuous variables with normal distribution and homogeneity of variance, Student's *t*-test was used to compare the differences between the two groups; one-way ANOVA was used to compare the differences with one variable among multiple groups; two-way ANOVA was used to compare the differences with two variables among multiple groups. P<0.05 was considered statistically significant, and statistical significance was defined as * P<0.05, ** P<0.01, *** P<0.001, **** P<0.0001, and "ns" indicated statistical non-significance.

Compliance and ethics

The author(s) declare that they have no conflict of interest. The Ethics Committee of Peking University Cancer Hospital and Institute approved all procedures performed in studies involving human participants (2020KT50) and were by the 1964 Helsinki Declaration and its later amendments or comparable ethical standards. All animal protocols were approved by the Animal Care and Use Committee of the Peking University Cancer Hospital & Institute (EAEC 2018-11).

Acknowledgement

This work was supported by the National Natural Science Foundation of China (81972842, 82373082, 81988101, 82173152).

References

Aguilar, R., Spencer, K.B., Kesner, B., Rizvi, N.F., Badmalia, M.D., Mrozowich, T., Mortison, J.D., Rivera, C., Smith, G.F., Burchard, J., et al. (2022). Targeting Xist with compounds that disrupt RNA structure and X inactivation. Nature 604, 160–166.

Ambardekar, V.V., Han, H.Y., Varney, M.L., Vinogradov, S.V., Singh, R.K., and Vetro, J.A. (2011). The modification of siRNA with 3′ cholesterol to increase nuclease protection and suppression of native mRNA by select siRNA polyplexes. Biomaterials 32, 1404–1411.

Arena, G., Cissé, M.Y., Pyrdziak, S., Chatre, L., Riscal, R., Fuentes, M., Arnold, J.J., Kastner, M., Gayte, L., Bertrand-Gaday, C., et al. (2018). Mitochondrial MDM2 regulates respiratory complex I activity independently of p53. Mol Cell 69, 594–609.e8.

Aviñó, A., Clua, A., Bleda, M.J., Eritja, R., and Fàbrega, C. (2021). Evaluation of floxuridine oligonucleotide conjugates carrying potential enhancers of cellular uptake. Int J Mol Sci 22, 5678.

Bhola, N.E., Balko, J.M., Dugger, T.C., Kuba, M.G., Sánchez, V., Sanders, M., Stanford, J., Cook, R.S., and Arteaga, C.L. (2013). TGF-β inhibition enhances chemotherapy action against triple-negative breast cancer. J Clin Invest 123, 1348–1358.

Brown, C.R., Gupta, S., Qin, J., Racie, T., He, G., Lentini, S., Malone, R., Yu, M., Matsuda, S., Shulga-Morskaya, S., et al. (2020). Investigating the pharmacodynamic durability of GalNAc-siRNA conjugates. Nucleic Acids Res 48, 11827–

11844.
Carilla-Latorre, S., Annesley, S.J., Muñoz-Braceras, S., Fisher, P.R., and Escalante, R. (2013). Ndufaf5 deficiency in the Dictyostelium model: new roles in autophagy and development. Mol Biol Cell, 24, 1519–1528.
Cathomas, R., Lorch, A., Bruins, H.M., Compérat, E.M., Cowan, N.C., Efstathiou, J.A., Fietkau, R., Gakis, G., Hernández, V., Espinós, E.L., et al. (2022). The 2021 updated European Association of Urology guidelines on metastatic urothelial carcinoma. Eur Urol 81, 95–103.
Choi, H.J., Jhe, Y.L., Kim, J., Lim, J.Y., Lee, J.E., Shin, M.K., and Cheong, J.H. (2020). FoxM1-dependent and fatty acid oxidation-mediated ROS modulation is a cell-intrinsic drug resistance mechanism in cancer stem-like cells. Redox Biol 36, 101589.
Davis, M.E., Zuckerman, J.E., Choi, C.H.J., Seligson, D., Tolcher, A., Alabi, C.A., Yen, Y., Heidel, J.D., and Ribas, A. (2010). Evidence of RNAi in humans from systemically administered siRNA via targeted nanoparticles. Nature 464, 1067–1070.
Ding, X.Y., Hu, H.Y., Huang, K.N., Wei, R.Q., Min, J., Qi, C., Tang, H., and Qin, X. (2020). Ubiquitination of NOTCH2 by DTX3 suppresses the proliferation and migration of human esophageal carcinoma. Cancer Sci 111, 489–501.
Elbashir, S.M., Harborth, J., Lendeckel, W., Yalcin, A., Weber, K., and Tuschl, T. (2001). Duplexes of 21-nucleotide RNAs mediate RNA interference in cultured mammalian cells. Nature 411, 494–498.
Fiedorczuk, K., and Sazanov, L.A. (2018). Mammalian mitochondrial complex I structure and disease-causing mutations. Trends Cell Biol 28, 835–867.
Fu, H., Zhang, Z., Li, D., Lv, Q., Chen, S., Zhang, Z., and Wu, M. (2022). LncRNA *PELATON*, a ferroptosis suppressor and prognositic signature for GBM. Front Oncol 12, 817737.
Galsky, M.D., Hahn, N.M., Rosenberg, J., Sonpavde, G., Hutson, T., Oh, W.K., Dreicer, R., Vogelzang, N., Sternberg, C.N., Bajorin, D.F., et al. (2011). Treatment of patients with metastatic urothelial cancer "Unfit" for cisplatin-based chemotherapy. J Clin Oncol 29, 2432–2438.
Gong, N., Teng, X., Li, J., and Liang, X.J. (2019). Antisense oligonucleotide-conjugated nanostructure-targeting lncRNA MALAT1 Inhibits cancer metastasis. ACS Appl Mater Interfaces 11, 37–42.
Gupta, R.A., Shah, N., Wang, K.C., Kim, J., Horlings, H.M., Wong, D.J., Tsai, M.C., Hung, T., Argani, P., Rinn, J.L., et al. (2010). Long non-coding RNA HOTAIR reprograms chromatin state to promote cancer metastasis. Nature 464, 1071–1076.
Gwon, Y., Maxwell, B.A., Kolaitis, R.M., Zhang, P., Kim, H.J., and Taylor, J.P. (2021). Ubiquitination of G3BP1 mediates stress granule disassembly in a context-specific manner. Science 372, eabf6548.
Hanna, N., Johnson, D., Temin, S., Baker Jr, S., Brahmer, J., Ellis, P.M., Giaccone, G., Hesketh, P.J., Jaiyesimi, I., Leighl, N.B., et al. (2017). Systemic therapy for stage IV non-small-cell lung cancer: american society of clinical oncology clinical practice guideline update. J Clin Oncol 35, 3484–3515.
He, P., Zhang, C., Chen, G., and Shen, S. (2021). Loss of lncRNA SNHG8 promotes epithelial-mesenchymal transition by destabilizing CDH1 mRNA. Sci China Life Sci 64, 1858–1867.
Huang, Y., Zheng, S., Guo, Z., de Mollerat du Jeu, X., Liang, X.J., Yang, Z., Zhang, H. Y., Gao, S., and Liang, Z. (2022). Ionizable liposomal siRNA therapeutics enables potent and persistent treatment of Hepatitis B. Sig Transduct Target Ther 7, 38.
Kanasty, R., Dorkin, J.R., Vegas, A., and Anderson, D. (2013). Delivery materials for siRNA therapeutics. Nat Mater 12, 967–977.
Lee, K., Giltnane, J.M., Balko, J.M., Schwarz, L.J., Guerrero-Zotano, A.L., Hutchinson, K.E., Nixon, M.J., Estrada, M.V., Sánchez, V., Sanders, M.E., et al. (2017). MYC and MCL1 cooperatively promote chemotherapy-resistant breast cancer stem cells via regulation of mitochondrial oxidative phosphorylation. Cell Metab 26, 633–647. e7.
Li, G., Li, X., Zhuang, S., Wang, L., Zhu, Y., Chen, Y., Sun, W., Wu, Z., Zhou, Z., Chen, J., et al. (2022). Gene editing and its applications in biomedicine. Sci China Life Sci 65, 660–700.
Li, X., Wu, Z., Wang, Y., Mei, Q., Fu, X., and Han, W. (2013). Characterization of adult α- and β-globin elevated by hydrogen peroxide in cervical cancer cells that play a cytoprotective role against oxidative insults. PLOS ONE 8, e54342.
Li, Y., Ding, J., Xu, X., Shi, R., Saw, P.E., Wang, J., Chung, S., Li, W., Aljaeid, B.M., Lee, R.J., et al. (2020). Dual hypoxia-targeting RNAi nanomedicine for precision cancer therapy. Nano Lett 20, 4857–4863.
Ma, Y., Chen, H., Su, S., Wang, T., Zhang, C., Fida, G., Cui, S., Zhao, J., and Gu, Y. (2015). Galactose as broad ligand for multiple tumor imaging and therapy. J Cancer 6, 658–670.
Matsui, M., and Corey, D.R. (2017). Non-coding RNAs as drug targets. Nat Rev Drug Discov 16, 167–179.
Nair, J.K., Attarwala, H., Sehgal, A., Wang, Q., Aluri, K., Zhang, X., Gao, M., Liu, J., Indrakanti, R., Schofield, S., et al. (2017). Impact of enhanced metabolic stability on pharmacokinetics and pharmacodynamics of GalNAc-siRNA conjugates. Nucleic Acids Res 45, 10969–10977.
Newby, G.A., Yen, J.S., Woodard, K.J., Mayuranathan, T., Lazzarotto, C.R., Li, Y., Sheppard-Tillman, H., Porter, S.N., Yao, Y., Mayberry, K., et al. (2021). Base editing of haematopoietic stem cells rescues sickle cell disease in mice. Nature 595, 295–302.
NSCLC Meta-analysis Collaborative Group. (2014). Preoperative chemotherapy for non-small-cell lung cancer: a systematic review and meta-analysis of individual participant data. Lancet 383, 1561–1571.
Pan, Y., Lu, X., Shu, G., Cen, J., Lu, J., Zhou, M., Huang, K., Dong, J., Li, J., Lin, H., et al. (2023). Extracellular vesicle-mediated transfer of lncRNA *IGFL2-AS1* confers sunitinib resistance in renal cell carcinoma. Cancer Res 83, 103–116.
Paschen, S.A., and Neupert, W. (2001). Protein import into mitochondria. IUBMB Life 52, 101–112.
Patil, D.P., Chen, C.K., Pickering, B.F., Chow, A., Jackson, C., Guttman, M., and Jaffrey, S.R. (2016). m^{6}A RNA methylation promotes *XIST*-mediated transcriptional repression. Nature 537, 369–373.
Paudel, R.R., Lu, D., Roy Chowdhury, S., Monroy, E.Y., and Wang, J. (2023). Targeted protein degradation via lysosomes. Biochemistry 62, 564–579.
Petrov, R.A., Mefedova, S.R., Yamansarov, E.Y., Maklakova, S.Y., Grishin, D.A., Lopatukhina, E.V., Burenina, O.Y., Lopukhov, A.V., Kovalev, S.V., Timchenko, Y. V., et al. (2021). New small-molecule glycoconjugates of docetaxel and GalNAc for targeted delivery to hepatocellular carcinoma. Mol Pharm 18, 461–468.
Pignata, S., C Cecere, S., Du Bois, A., Harter, P., and Heitz, F. (2017). Treatment of recurrent ovarian cancer. Ann Oncol 28, viii51–viii56.
Pillai, A.S., Chandler, S.A., Liu, Y., Signore, A.V., Cortez-Romero, C.R., Benesch, J.L.P., Laganowsky, A., Storz, J.F., Hochberg, G.K.A., and Thornton, J.W. (2020). Origin of complexity in haemoglobin evolution. Nature 581, 480–485.
Qi, X., Chen, S., He, H., Wen, W., and Wang, H. (2021). The role and potential application of extracellular vesicles in liver cancer. Sci China Life Sci 64, 1281–1294.
Shah, N., and Sukumar, S. (2010). The Hox genes and their roles in oncogenesis. Nat Rev Cancer 10, 361–371.
Shi, Q., Li, Y., Li, S., Jin, L., Lai, H., Wu, Y., Cai, Z., Zhu, M., Li, Q., Li, Y., et al. (2020). LncRNA DILA1 inhibits Cyclin D1 degradation and contributes to tamoxifen resistance in breast cancer. Nat Commun 11, 5513.
Sirnaomics, Inc. (2020). Sirnaomics announces positive topline results from interim analysis of ongoing phase II clinical trial evaluating STP705 in cutaneous squamous cell carcinoma *in situ* (isSCC) (FirstWord Pharma).
Stine, Z.E., Schug, Z.T., Salvino, J.M., and Dang, C.V. (2022). Targeting cancer metabolism in the era of precision oncology. Nat Rev Drug Discov 21, 141–162.
Sugiana, C., Pagliarini, D.J., McKenzie, M., Kirby, D.M., Salemi, R., Abu-Amero, K.K., Dahl, H.H.M., Hutchison, W.M., Vascotto, K.A., Smith, S.M., et al. (2008). Mutation of *C20orf7* disrupts complex I assembly and causes lethal neonatal mitochondrial disease. Am J Hum Genet 83, 468–478.
Sun, P., Han, Y., Zhu, Y., Hu, K., Huang, S., Tan, J., Wang, M., Wu, H., and Tang, G. (2020). RETRACTED: radiosynthesis and biological evaluation of fluorine-18 labeled *N*-acetylgalactosamine derivative [^{18}F]FPGalNAc for PET imaging of asialoglycoprotein receptor-positive tumors. Nucl Med Biol 88–89, 1–9.
Tsai, M.C., Manor, O., Wan, Y., Mosammaparast, N., Wang, J.K., Lan, F., Shi, Y., Segal, E., and Chang, H.Y. (2010). Long noncoding RNA as modular scaffold of histone modification complexes. Science 329, 689–693.
Viney, N.J., van Capelleveen, J.C., Geary, R.S., Xia, S., Tami, J.A., Yu, R.Z., Marcovina, S.M., Hughes, S.G., Graham, M.J., Crooke, R.M., et al. (2016). Antisense oligonucleotides targeting apolipoprotein(a) in people with raised lipoprotein(a): two randomised, double-blind, placebo-controlled, dose-ranging trials. Lancet 388, 2239–2253.
Wang, S., Yu, G., Wang, Z., Jacobson, O., Lin, L.S., Yang, W., Deng, H., He, Z., Liu, Y., Chen, Z.Y., et al. (2019). Enhanced antitumor efficacy by a cascade of reactive oxygen species generation and drug release. Angew Chem Int Ed 58, 14758–14763.
Wang, Y Q., Wang, X., Yan, S., Yang, Y., and Wu, N. (2017). Progress of neoadjuvant therapy combined with surgery in non-small cell lung cancer (in Chinese). Chinese Journal of Lung Cancer, 20, 352–360.
West, A.P., Brodsky, I.E., Rahner, C., Woo, D.K., Erdjument-Bromage, H., Tempst, P., Walsh, M.C., Choi, Y., Shadel, G.S., and Ghosh, S. (2011). TLR signalling augments macrophage bactericidal activity through mitochondrial ROS. Nature 472, 476–480.
Winkle, M., El-Daly, S.M., Fabbri, M., and Calin, G.A. (2021). Noncoding RNA therapeutics—challenges and potential solutions. Nat Rev Drug Discov 20, 629–651.
Xu, X., Wang, C., Zhang, P., Gao, X., Guan, W., Wang, F., Li, X., Yuan, J., Dou, H., and Xu, G. (2022). Enhanced intracellular reactive oxygen species by photodynamic therapy effectively promotes chemoresistant cell death. Int J Biol Sci 18,

374–385.
Yang, F., Hu, A., Guo, Y., Wang, J., Li, D., Wang, X., Jin, S., Yuan, B., Cai, S., Zhou, Y., et al. (2021). p113 isoform encoded by CUX1 circular RNA drives tumor progression via facilitating ZRF1/BRD4 transactivation. Mol Cancer 20, 123.
Yu, J., Zhu, C., Wang, X., Kim, K.J., Bartolome, A., Dongiovanni, P., Yates, K.P., Valenti, L., Carrer, M., Sadowski, T., et al. (2021). Hepatocyte TLR4 triggers inter-hepatocyte Jagged1/Notch signaling to determine NASH-induced fibrosis. Sci Transl Med 13, eabe1692.
Yuan, J., Yue, H., Zhang, M., Luo, J., Liu, L., Wu, W., Xiao, T., Chen, X., Chen, X., Zhang, D., et al. (2016). Transcriptional profiling analysis and functional prediction of long noncoding RNAs in cancer. Oncotarget 7, 8131–8142.
Zhang, C., Xu, C., Gao, X., and Yao, Q. (2022a). Platinum-based drugs for cancer therapy and anti-tumor strategies. Theranostics 12, 2115–2132.
Zhang, C., and Zhang, B. (2023). RNA therapeutics: updates and future potential. Sci China Life Sci 66, 12–30.
Zhang, H., Xu, R., Li, B., Xin, Z., Ling, Z., Zhu, W., Li, X., Zhang, P., Fu, Y., Chen, J., et al. (2022b). LncRNA NEAT1 controls the lineage fates of BMSCs during skeletal aging by impairing mitochondrial function and pluripotency maintenance. Cell Death Differ 29, 351–365.
Zhang, J., Kay, M.K., Park, M.H., Meruvu, S., Powell, C., and Choudhury, M. (2022c). LncRNA DLEU2 regulates sirtuins and mitochondrial respiratory chain complex IV: a novel pathway in obesity and offspring's health. Int J Obes 46, 969–976.
Zhang, M., Zhang, B., Wang, X., Song, J., Tong, M., Dong, Z., Xu, J., Liu, M., Jiang, Y., Wang, N., et al. (2023). LncRNA CFAR promotes cardiac fibrosis via the miR-449a-5p/LOXL3/mTOR axis. Sci China Life Sci 66, 783–799.
Zhang, Q., Li, D., Dong, X., Zhang, X., Liu, J., Peng, L., Meng, B., Hua, Q., Pei, X., Zhao, L., et al. (2022d). LncDACH1 promotes mitochondrial oxidative stress of cardiomyocytes by interacting with sirtuin3 and aggravates diabetic cardiomyopathy. Sci China Life Sci 65, 1198–1212.
Zheng, M., Liu, Y., Wang, Y., Zhang, D., Zou, Y., Ruan, W., Yin, J., Tao, W., Park, J.B., and Shi, B. (2019). ROS-responsive polymeric siRNA nanomedicine stabilized by triple interactions for the robust glioblastoma combinational RNAi therapy. Adv Mater 31, e1903277.
Zheng, Y., Miyamoto, D.T., Wittner, B.S., Sullivan, J.P., Aceto, N., Jordan, N.V., Yu, M., Karabacak, N.M., Comaills, V., Morris, R., et al. (2017). Expression of β-globin by cancer cells promotes cell survival during blood-borne dissemination. Nat Commun 8, 14344.
Zhu, H., Zhang, L., Yan, S., Li, W., Cui, J., Zhu, M., Xia, N., Yang, Y., Yuan, J., Chen, X., et al. (2017). LncRNA16 is a potential biomarker for diagnosis of early-stage lung cancer that promotes cell proliferation by regulating the cell cycle. Oncotarget 8, 7867–7877.
Zou, Y., Sun, X., Wang, Y., Yan, C., Liu, Y., Li, J., Zhang, D., Zheng, M., Chung, R.S., and Shi, B. (2020). Single siRNA nanocapsules for effective siRNA brain delivery and glioblastoma treatment. Adv Mater 32, e2000416.